PERFORMANCE OF FRP-STRENGTHENED REINFORCED CONCRETE BEAMS SUBJECTED TO LOW TEMPERATURE

by

Emtiaz Ahmed

A thesis submitted in partial fulfillment
of the requirements for the degree

of

Master of Science

in

Civil Engineering

MONTANA STATE UNIVERSITY
Bozeman, Montana

May 2021

ACKNOWLEDGEMENTS

The completion of this study owes immensely to the whole-hearted assistance and cordial cooperation in different ways by many people. Firstly, I would like to express my utmost gratitude to my advisor, Dr. Kirsten Matteson, for her kind supervision and guidance throughout my thesis work and her assistance in different academic issues during my master program. I would like to give the sincerest appreciation and kind gratitude to Dr. Michael Berry, who took time to help in testing and for his critical input to this study.

I am also thankful to Dr. Ladean McKittrick and Mr. Dan Samborsky for their contributions to my research. I also thank my committee member Dr. Damon Fick for his time and assistance in my coursework and research.

Graduate researchers Daniel Malyuta, Jaden Stewart, and undergrad researchers James Starke, Ethan Turner, Amanda Williams helped me in casting and testing the specimen for this study and I thank them for their effort. Finally, I want to thank two of my friends Musaddeque A Syed and Kazi Tahsin Huda for their time and assistance in many ways to this work.

TABLE OF CONTENTS

TABLE OF CONTENTS CONTINUED

LIST OF TABLES

Table Page

LIST OF TABLES CONTINUED

Table Page

LIST OF FIGURES

Figure Page

LIST OF FIGURES CONTINUED

Figure Page

LIST OF FIGURES CONTINUED

Figure Page

LIST OF FIGURES CONTINUED

Figure Page

NOMENCLATURE

Ψ_f = Reduction factor.

α_1 = Stress block factor.

β_1 = Ratio of depth of equivalent rectangular stress block to depth of neutral axis.

ε_{bi} = Strain in concrete substrate at time of FRP installation.

ε_c = Concrete strain at extreme concrete compression fiber.

ε_c' = Strain corresponding to the compressive strength of concrete, f_c'.

ε_{fd} = Debonding strain of FRP.

ε_{fe} = Effective strain of FRP.

ε_{fu} = FRP strain.

ε_s = Strain in tension reinforcement.

ε'_s = Strain in compression reinforcement.

a = Depth of the Whitney stress block.

b = Width.

b_f = Width of FRP.

c = Distance from extreme compression fiber to neutral axis.

d = Distance from extreme compression fiber to centroid of tension reinforcement.

d' = Distance from extreme compression fiber to centroid of compression reinforcement.

d_f = Effective depth of FRP.

f'_c = Compressive strength of concrete.

f_r = Modulus of rupture.

NOMENCLATURE CONTINUED

f_s = Stress in tension reinforcement.

f'_s = Stress in compression reinforcement.

f_{su} = FRP stress.

f_y = Yield stress of reinforcement.

h = Height.

n = Number of FRP layer.

t_f = Thickness of FRP.

y_t = Centroid.

A_s = Area of reinforcement in tension zone.

A'_s = Area of reinforcement in compression zone.

C_c = Compression force in concrete.

C_E = Environmental factor.

C_s = Compression force in reinforcement.

E_f = Modulus of elasticity of the FRP.

E_y = Modulus of elasticity of reinforcement.

F = Applied load.

I_g = Gross moment of inertia.

L = Span length.

M = Bending moment.

M_{cr} = Cracking moment.

NOMENCLATURE CONTINUED

M_n = Nominal moment strength.

M_{nf} = Contribution of FRP to nominal flexural strength.

M_{ns} = Contribution of steel reinforcement to nominal flexural strength.

P = Ultimate load carrying capacity.

T = Tension force in reinforcement.

V = Shear force.

ABSTRACT

The use of Fiber Reinforced Polymer (FRP) to repair and strengthen existing concrete structural elements (beams, columns, beam-column connections, and slabs) has become globally accepted and popular. FRP can be used for this application in several forms, such as externally applied wrapping, Near Surface Mounted (NSM) bars, lamination, and sheets. The strength to weight ratio of this material is one of the main criteria that makes this material approved and desired by engineers and researchers for this application. Also, FRP is corrosion resistant and requires less installation time compared to other repairing techniques such as jacketing, section enlargement, and external post tensioning. The performance of FRP repairs has been studied extensively at conventional, non-extreme temperatures; however, little research has been conducted on the performance of these repairs at cold temperatures. The research discussed herein aims to fill this gap in knowledge so that FRP repairs can be more widely used in cold temperature environments, such as for bridge repairs in the state of Montana.

In this work, six beams (6 in. × 8 in., 10 ft long) were constructed and tested in four-point bending at two different temperatures (room temperature and -40^{o}C). For each temperature, there were three beam types: 1) a control beam, 2) a longitudinal strengthened beam, and 3) a longitudinal + transverse strengthened beam. Overall, the results showed that low temperatures have a generally positive effect on concrete strength and beam performance. The average concrete compressive strength of frozen cylinders at -40^{o} C was observed to be 87.18% higher than the cylinders tested at room temperature. For all beam types, the ultimate load carrying capacity of the low temperature beams exceeded the capacity of the counterpart beam tested at room temperature. Additionally, at lower temperatures the strengthened beams showed delayed FRP delamination (occurring at higher displacements). Further, the initial stiffnesses of the cold beams were found to be significantly higher than the room temperature beams. Overall, the results of this study are promising for the potential of use of FRP for repairs in cold environments and future research is warranted.

KEYWORDS: fiber reinforced polymer (FRP) repairs, strengthened reinforced concrete (RC) beams, low temperature structural testing, FRP delamination.

CHAPTER ONE

INTRODUCTION

Background

Reinforced concrete (RC) structures have been constructed over the years, all over the world. Older structures, following older design codes, may not satisfy current design requirements or today's increased loading demands. Additionally, concrete structures can degrade over time because of sustained load, corrosion, and exposure to challenging weather. It is not always ideal (or in some cases possible) to replace existing structures because of economic and technical constraints. To increase the safety and life span of these structures, it can be necessary to repair, strengthen, and/or rehabilitate instead of replacing. There are several methods of strengthening existing structures, such as external use of Fiber Reinforced Polymer (FRP), concrete jacketing, bonded steel elements, and external post-tensioning, among others. The concern when strengthening existing structures is to choose the suitable method(s) that meet the required criteria, such as availability, budget, constructability, and other technical issues.

Motivation

FRP is becoming popular among design engineers because of its high strength to weight ratio, decreased production and installation time, and corrosion resistance. In recent years, FRP has been widely used to reinforce concrete; it has been used in new construction, as a repair material, and for external strengthening of existing elements. Significant research on strengthening structural elements (beams, columns, and slabs) has been conducted at room temperatures. Despite

the proven advantages of using FRPs over traditional materials at room temperatures, little is known about its performance at low temperatures, thus hindering its widespread use in cold climate regions.

Overall Scope and Research Objective

To fill this gap, the present study aims to observe the flexural performance of FRP strengthened RC beams in both room temperature and cold temperature (-40^{o}C) conditions under four-point bending tests. There are three beam types for each temperature condition (for a total of six beams): 1) control beams with no FRP strengthening, 2) longitudinal strengthened beams, and 3) longitudinal + transverse strengthened beams. For the longitudinal strengthened beams, one carbon FRP layer was applied. For the longitudinal + transverse strengthened beams, one carbon FRP layer was applied in the longitudinal direction and fourteen glass FRP layers were applied at 4 in. edge to edge distance in the transverse direction.

The overall objective of this research was to evaluate the performance (load-deflection responses) of FRP strengthened RC beams at both temperatures to compare results (ultimate capacity, failure mode, stiffness, etc.) and make conclusions about the potential for FRP to strengthen existing RC beams in cold environments. Additionally, the different FRP strengthening methods will be assessed; for example, the effects of transverse wrapping on the delamination process of the longitudinal FRP will be observed. Overall, this research will evaluate the potential for FRP repairs to be used in cold temperature applications, such as bridge beams in Montana.

Organization

A literature review of previous research is included in Chapter 2, including studies on 1) repair and strengthening methods of different concrete structural elements using FRP, 2) their applications on real structures, and 3) work that has been done with FRP in low temperatures. Chapter 3 provides a brief description of the materials used in this study. Chapter 4 discusses the material property testing conducted for this study and the results, including concrete cylinder and FRP coupon tests. Chapter 5 discusses the experimental design and test setup used in this study for the RC beams, along with experimental results, which include a comparison of behaviors between control and strengthened beams in both temperature conditions. Chapter 6 summarizes the conclusions drawn and discusses future recommendations for the research. There are also three Appendices that provide additional details on specific aspects of the research.

CHAPTER TWO

LITERATURE REVIEW

Introduction

This chapter briefly discusses real-world structural applications of different methods and applications of various FRP strengthening techniques, broken down by global and US applications. An overview on previous research on the external wrapping method (method used for this thesis research) is also provided and the results and significance of these research efforts are also discussed. Research efforts on low temperature conditions are also presented and discussed in this thesis since the behavior of FRP strengthened concrete members subjected to low temperatures is a concern of this present study.

Methods and Applications of FRP Strengthening

The strengthening of existing concrete structures with FRP is a comparatively newer technique in the strengthening and repairing sector, but it has become very popular and globally accepted by structural engineers and researchers over the years. Several research works on different methods of applying FRP, including lamination, Near Surface Mounted (NSM) bar, and external wrapping with epoxy, have been performed in different conditions. FRP wrapping externally with epoxy resin by the wet layup method was used for this thesis work and applicable research efforts will be discussed in more detail later in this chapter. A brief overview of the research performed with the other methods is included here.

Strengthening existing concrete structures with FRP laminates includes preparing the concrete surface and attaching FRP laminates to the concrete with an epoxy resin system. Anchorage is often used at different locations (primarily at the ends) to grip the FRP sheets (Julio et al. 2006, El-Hacha et al. 2004). Significant works using the lamination method have been focused on strengthened beams (Morsy and Mahmoud 2012, Hosny et al. 2006, Wenwei and Guo 2006) and strengthened columns (Ehsani et al. 2012, Sadone et al. 2013).

Near Surface Mounted (NSM) is another form of FRP strengthening, which is a comparatively newer technique among the FRP application methods. Aiswarya and Prabhakaran (2017) described the NSM technique as cutting a series of shallow channels on concrete or masonry surfaces in the desired direction and then placing reinforcements into the channels after partially filling with epoxy mortar. This technique has been used for strengthening beams (Khalifa 2016, Chołostiakow and Kotynia 2014, Hosen et al. 2016), columns (Sarfaraz and Danesh 2011), and beam-column connections (Prota et al. 2000).

As stated previously, FRP repairs have gained attention globally and an overview of the global applications on bridge projects of different forms of FRP used to repair real structures is presented in Table 1.

Table 1. Worldwide applications of FRP strengthening systems on bridge projects.

Title/Project name	**Authors/ Organization**	**Year**	**Bridge name, Country**	**Applications**
Application of FRP bars as reinforcement in civil engineering structures	R.V. Balendran T.M. Rana T. Maqsood W.C. Tang	2002	Oppegaard footbridge, Norway	Glass FRP straight rods were used to provide stability to bridge beams.
Advances in the application of FRP	R. Sen	2003	Highway 10, Quebec, Canada	Carbon fiber and glass fiber wrap were provided to strengthen corrosion-

for repairing corrosion damage				damaged circular columns (in 1996).
			Champlain bridge, Montreal, Canada	Fiberglass type E (SEH51/TYFO S) wrap was used to regain initial strength of corroded RC piers (in 1996).
			Leslie Street Bridge, Toronto, Canada	Glass fiber and aramid fiber were used to repair the damaged column of Leslie Street Bridge.
Case Study of Application of FRP Composites in Strengthening the Reinforced Concrete Headstock of a Bridge Structure	A. Nezamian S. Setunge	2004	Tenthill Bridge, Australia	CFRP strengthening system was used to increase the flexural capacity of bridge beam and the shear capacity of headstock.
FRP: Research, Education and Application in India and China in Civil Engineering	R. Shrivastava U. Gupta U. B Choubey	2009	Highway bridge in Miyun, China	Bridge beam was upgraded to GFRP composite beam after being unstable one year after construction. (in 1987)
Purfleet Footbridge	Life span structures ltd.	2013	Purfleet Footbridge, United Kingdom	The existing deteriorated timber footbridge was replaced by FRP composite bridge decks which weighs about a third of the equivalent steel option.
Deck replacement using GFRP and CFRP pultrusion (Church Road Bridge)	Composites UK	2014	Church Road Bridge, United Kingdom	GFRP and CFRP pultrusion elements were used to replace the main deck of the bridge.
Use of FRP composite for strengthening of concrete structures	Z. Abbas F. Shahadat	2015	Chaltan Bridge, India	FRP reinforcement by Wet-Layup process was applied to the bridge beams to increase shear and flexural capacity.

The key takeaways from the studies listed in Table 1 that included post repair inspection results include:

- No significant corrosion problems have been found since repairs took place (Sen, R 2003).
- Since upgrades, the Miyun bridge did not show any major stability problems (Shrivastava et al 2009).

In the early 1970s, the United States started showing interest in using FRP materials in bridge construction and repair projects (McCormick 1972). In the late 1980s, the Federal Highway Administration (FHWA) and the National Science Foundation (NSF) began increasing funding to enable research on FRP materials for infrastructure applications after observing the growing acceptance of advanced composite materials in different fields (e.g. sporting goods and aerospace industries) and the potential FRP has as a corrosion resistant construction material (Bank 2006). Therefore, since the late 1980s, increased research and development has led to the introduction of FRP materials being used in pedestrian and vehicular bridges. Key applications in the United States are summarized in Table 2.

Table 2. United States applications of FRP strengthening systems on bridge projects.

Title	Authors	Year	Bridge name, State	Applications
Solid RC Decks Strengthened with FRP.	T. Alkhrdaji A. Nanni G. Chen M. Barker	1999	Bridge J-857, Missouri.	Externally bonded CFRP sheets and NSM CFRP rods were used to strengthen the bridge decks.
Repair of Corrosion-Damaged Columns Using FRP Wraps.	R. Harichandran M. Baiyasi	2000	Lansing road, under the I-96 overpass, Michigan.	Corrosion damaged columns were repaired by unidirectional GFRP and CFRP wrap.
Retrofit of Existing Reinforced Concrete	B. Shahrooz S. Boy	2001	Bridge CLI-380-0032,	CFRP plates were used as a

Bridges with Fiber Reinforced Polymer Composites.			Ohio.	strengthening material to increase the capacity of the bridge slab.
FRP Reinforced Concrete in Texas Transportation- Past, Present, Future. Field Applications of FRP Reinforcement: Case Studies.	T. Bradberry S. Wallace	2003	Farm-to-market bridge, Texas.	CFRP layer was used to repair and strengthen the bridge's beam, which was damaged by an over-height vehicle.
Flexural Strengthening of Impacted PC Girder with FRP Composites. Field Applications of FRP Reinforcement: Case Studies.	R. Parretti A. Nanni J. Cox C. Jones R. Mayo	2003	Bridge A5657, Missouri.	CFRP laminates and U-wrap were used as strengthening methods to hold together fractured tendons.
Repair of the Uphapee Creek Bridge with FRP Laminates	B. Carmichael, R. Barnes,	2005	Uphapee Creek bridge, Alabama.	Externally bonded FRP strips were provided to strengthen the bridge girders.
District 3-0 Investigation of Fiber-Wrap Technology for Bridge Repair and Rehabilitation (Phase-I).	J. Davalos K. Barth I. Ray C. Lin D. Brayack	2006	Alaskan Way Viaduct, Washington.	Carbon fiber wrap was used to reinforce the crossbeams and edge beams, damaged because of the Nisqually earthquake.
Retrofit of the Louisa-Fort Gay Bridge Using CFRP Laminates.	C. Choo T. Zhao I. Harik	2007	Louisa-Fort Gay bridge, Kentucky.	CFRP laminates were used to retrofit and improve the strength and stiffness of the girders.
Higgins Avenue Bridge Rehabilitation.	C. Kelly	2018	Higgins bridge, Montana.	Structural components were repaired using FRP and the bridge deck was replaced to extend the service life of the bridge.

Among the applications listed in Table 2, the studies that included post repair inspection results include Bridge CLI-380-0032, Ohio, Lansing road under the I-96 overpass, Michigan and Uphapee Creek bridge, Alabama. All three studies reported no significant problems and satisfactory performance since FRP strengthening occurred. Harichandran and Baiyasi (2000) brought up an important point that although the CFRP cost was about 40% higher, the repairs required one fewer layer because of its higher strength and stiffness than the GFRP.

Figures 1 and 2 show before and after pictures of a couple selected FRP repairs on bridge beams at different locations in the United States, previously listed in Table 2.

Figure 1. Louisa-Fort Gay bridge, Kentucky; before (a) and after (b) strengthening (Choo et al. 2007).

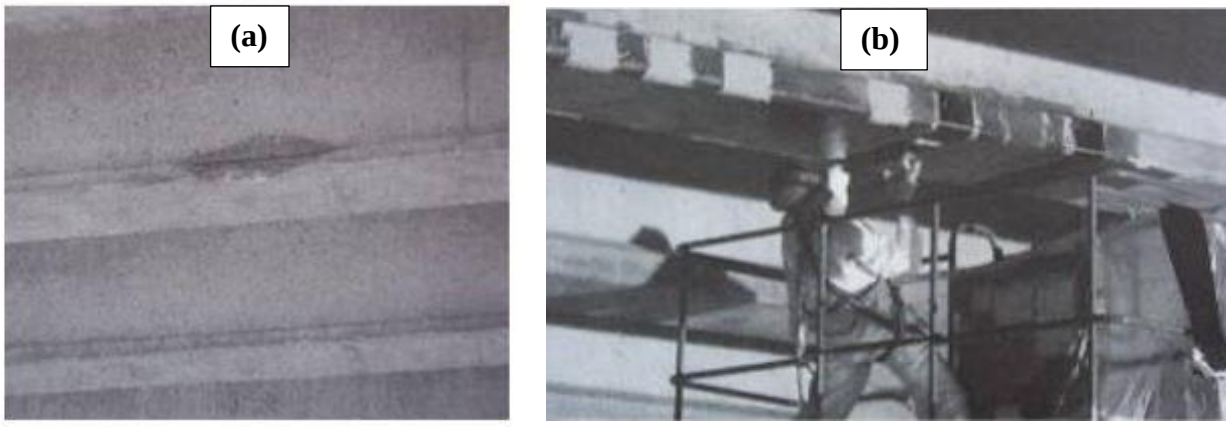

Figure 2. Bridge A5657, Missouri; before (a) and after (b) strengthening (Parretti et al. 2003).

External Wrapping

One of the most common methods of using FRP in the strengthening and repairing sector is external wrapping with epoxy resin. There are three main processes of applying FRP externally for strengthening: wet layup systems, prepreg systems, and precured systems (Julio et al. 2006, R. Sen. 2003). Among these methods, the wet layup method is most popular because of its easy application process and less time requirement, and is the method used in the current study. Several researchers used this method during their research (Ghaffary and Moustafa 2020, Julio et al. 2006, R. Sen. 2003, and Ehsani et al. 2012). The process can be briefly described with the following steps: surface preparation of the existing structure, application of epoxy resin to the surface, placing fiber fabrics to the structure surface, and application of epoxy resin on the fiber fabrics (see Figure 3, Ghaffary and Moustafa 2020). The detailed process of applying FRP by the wet layup method is also outlined in ACI 440.2R-17. One example highlighted here that employed this strengthening method was the repair work of the Chaltan bridge, India (Abbas and Shahadat 2015) and Figure 4 shows photographs of this work.

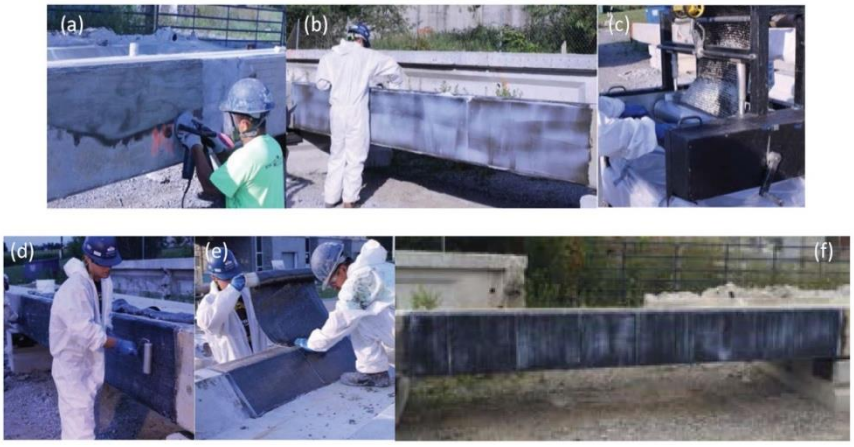

Figure 3. FRP application by wet layup method; surface preparation (a), epoxy application to concrete surface (b), placing FRP to structure surface and epoxy application (c, d, and e) and final FRP strengthened structure (f) (Ghaffary and Moustafa 2020).

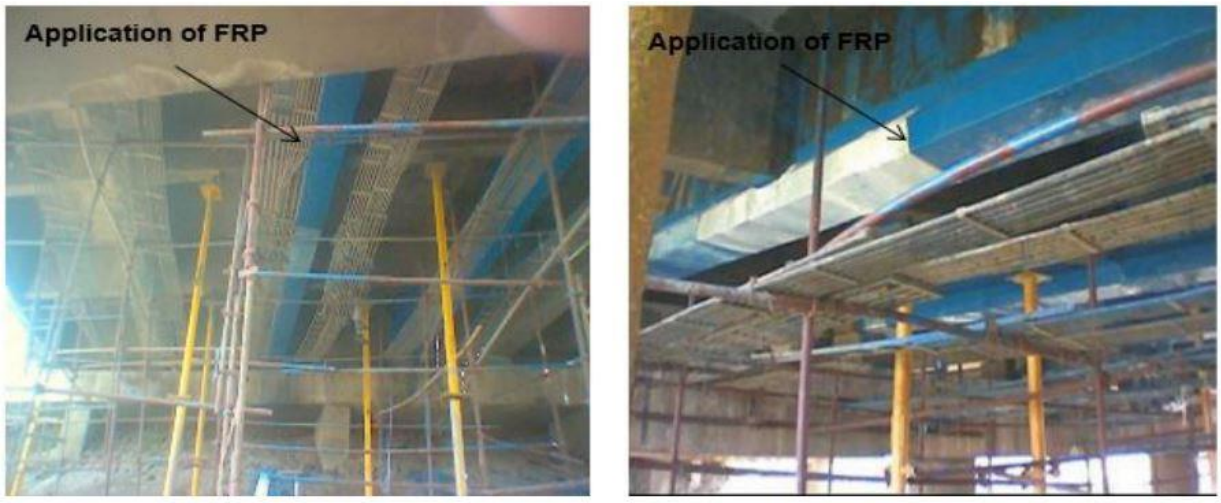

Figure 4. FRP application in Chaltan bridge, India (Abbas and Shahadat 2015).

For repairing and strengthening existing structures with external wrapping, layering of the FRP materials is a key factor in obtaining desired strength and performance (J.L et al. 2003, Hadi 2003) and the research performed for this thesis relied on investigating previous research to decide on the layering and strengthening schemes that would be studied here. For example, Sahawany et al. (1996) showed that one, two, and three layers of CFRP increased the cracking moment by 12%, 61%, and 105%, respectively, and deflection decreased inversely with increased number of CFRP layers. Additionally, Harichandran and Baiyasi (2000) stated that 2 layers of CFRP versus 3 layers of GFRP showed similar performance in corrosion resistance. One of the main concerns of applying FRP externally is delamination, and it has been shown that delamination risk can be reduced by applying additional layering in the transverse direction (Pham and Hao 2016). Previously, Pham and Hao (2016) described eliminating stress concentrations and thus improving the strengthening effectiveness, as well as delaying premature debonding. The researchers used both longitudinal FRP for flexural resistance and transverse FRP for resistance to premature debonding. They tested different numbers of layers of CFRP for the strengthening scheme. Hosney

et al. (2006), Attari et al. (2012) and Hawileh et al. (2014) also tested different hybrid strengthening schemes (CFRP+GFRP). Tables 3 and 4 show the wrapping schemes used by Pham and Hao (2016) and Attari et al. (2012), respectively, two studies of particular interest for the current research.

Table 3. Beam type and wrapping scheme of "Impact Behavior of FRP-Strengthened RC Beams without Stirrups" (Pham and Hao 2016).

Beam	Section	Longitudinal FRP (layers)	Transverse FRP (wraps)	Shear capacity (kN)	Flexural capacity (kNm)
R	Rectangular	-	-	93	21
N-L1	Rectangular	1	-	93	23
N-L2T2	Rectangular	2	2	93	25
N-L2T7	Rectangular	2	7	123	25
M-L2T2	Modified	2	2	93	25
M-L2T7	Modified	2	7	93	25

Table 4. Beam type and wrapping scheme of "Flexural strengthening of concrete beams using CFRP, GFRP and hybrid FRP sheets" (Attari et al. 2012).

Beam No.		Strengthening schemes	Type of strengthening	FRP area m^2
	PC		Control specimen	–
Serial A	PA1	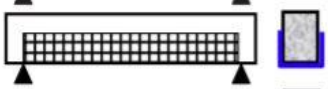	CFRP Wrap 1 Layers 0° and 1 layer 90°U Shape	0.78 CFRP
	PA2	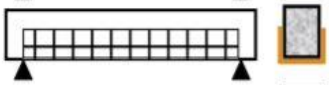	GFRP Wrap 2 Layers at 0° and 1 layer 90°U Shape	1.17 GFRP
	PA3		01 Layer GFRP 0° 01 Layer CFRP 0° U Shape	0.39 CFRP 0.39 GFRP
Serial B	PB4	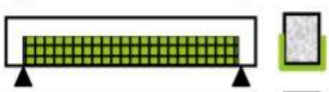	3 Layers HFRP U Shape	1.17 HFRP
	PB5	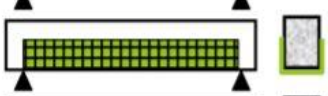	2 Layers HFRP U Shape	0.78 HFRP
	PB6		3 Layers HFRP	0.39 HFRP

Beam performances were observed under four-point bending by both Attari et al. (2012) and Hawileh et al. (2014), while Hosny et al. (2006) applied cyclic loading up to failure to observe the flexural behavior after strengthening. The four-point bending test set ups used by Attari et al. (2012) and Hawileh et al. (2014) are shown in Figures 5 and 6, respectively.

Figure 5. Four-point bending test set up used by Attari et al. (2012).

Figure 6. Four-point bending test set up used by Hawileh et al. (2014).

Overall, Attari et al. (2012) studied flexural behavior of FRP wrapped concrete beams using a hybrid strengthening scheme (CFRP + GFRP) and a U-anchorage strengthening configuration. They found a twin layer glass–carbon fibers composite material was very efficient for increasing strength capacity and the anchorage system improved the flexural strength. Overall, Pham and Hao (2016) showed the flexural behavior of two sets of FRP strengthened beams: 1) normal rectangular sections and 2) modified sections which were cast in special formwork, including a rectangular steel formwork and curved polystyrene foam formwork. The modified section eliminated the stress concentrations at the corners and showed higher load carrying capacity than that of normal-section beams by significantly delaying the debonding of the FRP. They concluded that the FRP U-wrap enhanced the capacity of the longitudinal wrapping.

Overall, the major research strategies and findings from these efforts that were useful to the present study include: 1) wrapping schemes for FRP flexural strengthening of beams, 2) FRP application method and 3) flexural test setup.

FRP Research Work in Low Temperatures

Some concrete structures that require strengthening and repairing have exposure to extreme environmental conditions, including corrosion potential environments and extreme cold climate conditions. Performance evaluation of the possible strengthening methods used on these structures is of utmost importance, and the focus of this thesis is FRP performance in cold temperatures, like Montana. Currently, very little research related to the performance of FRP strengthened structures in such extreme conditions has been done. Details of some related research works in this area are provided in Table 5.

Table 5. Research works on FRP strengthened concrete structures in low temperatures.

Title	Authors	Year	Overview and findings
Low temperature behaviour of concrete beams strengthened with FRP sheets.	M.E. Baumert M.F. Green M.A. Erki	1996	CFRP plated beams were exposed to a temperature difference of +21°C to –27°C and there were no adverse effects on the structural behavior of the beams when subjected to a static load.
Freeze-thaw durability of composite materials.	J. Gomez B. Casto	1996	Durability of CFRP externally attached to concrete beams exposed to freeze-thaw cycling was evaluated. No negative effects on ultimate load carrying capacity of the beams were found.
Performance of CFRP retrofitted concrete columns at low temperatures.	K.A. Soudki M. F. Green	1996	Behavior of CFRP wrapped concrete columns subjected to freeze-thaw were investigated. Strength increased by 20% and 30% for one layer and two layers of CFRP wrapping, respectively, at room temperature. With thermal cycling one layer of CFRP sheet tripled the beam strength compared to the unwrapped specimen.
Freeze-thaw response of CFRP wrapped concrete.	K.A. Soudki M. F. Green	1997	Freeze-thaw cycling had significant effect on the failure modes of FRP-wrapped specimens. They failed in a more brittle manner than similar specimens kept at room temperature.
Durability characteristics of concrete beams externally bonded with FRP composite sheets.	H.Toutanji T.El-Korchi	1998	Performance of concrete beams wrapped with GFRP sheets subjected to wet-dry and freeze-thaw cycling was evaluated. 20% and 5% reductions of strength of the GFRP wrapped specimen were found for wet-dry and freeze-thaw cycling, respectively.
Effect of freeze–thaw cycles on the bond durability between fibre reinforced polymer plate reinforcement and concrete.	M. F. Green L. A. Bisby, Y. Beaudoin P. Labossière	2000	The effects of 300 freeze–thaw cycles on the bond between CFRP strips and concrete beams were investigated. No reduction of load carrying capacity was found, but the FRP adhesion had been affected by freeze–thaw exposure.

Prestressed Carbon Fiber Reinforced Polymer Sheets for Strengthening Concrete Beams at Room and Low Temperatures.	R. El-Hacha, R. G. Wight M. F. Green	2004	Flexural behavior of pre-cracked concrete beams strengthened with bonded prestressed CFRP sheets were observed at both room temperature (+2°C) and cold temperature (-28°C). Cold temperature did not have adverse effects on the beam behavior.

Some studies shown in Table 5 indicate that freeze-thaw cycling does not cause significant deterioration of the load carrying capacity (Green et al. 2000, Baumert et al. 1996, Gomez and Casto 1996), but it has some effects on the failure modes of the specimens (Soudki and Green 1997) and the adhesion between the FRP and concrete (Green et al. 2000). Moreover, no adverse effects due to short exposure to cold temperatures were found on FRP strengthened beam flexural behavior (El-Hacha et al. 2004).

Bridge deterioration is a concern in Montana and FRP repairs (as opposed to total replacements) could be an economic option for the state in some cases. However, the behavior of FRP strengthened beams subjected to cold temperatures, tested under four-point bending, and the effects of exposure to cold temperatures on the delamination process of FRP are missing from the literature. This specific application of bridge beam FRP strengthening in cold temperatures is the focus of this thesis.

CHAPTER THREE

MATERIALS

Introduction

This chapter presents the concrete mix design used in this study. The material properties of the construction and strengthening materials used in this research are also discussed, including the yield strength of the rebar and the specifications of the fiber fabrics, epoxy resin, and thermocouple wire.

Concrete Mix Design

Concrete is traditionally composed of cement, water, aggregates, and admixtures. A concrete batch was mixed for each beam cast. The weights of the materials per cubic foot of concrete, are shown in Table 6.

Table 6. Weights of materials per cubic foot of concrete.

Material	**Weight per cubic foot**
Cement	22.76 lbs
Coarse aggregate	73.97 lbs
Fine aggregate	37.44 lbs
Water	12.68 lbs
Entrained air admixture	4.55 ml

The binder material, cement, comes from the GCC Trident Cement Plant and is Portland Cement, Type I/II/V. The properties of the cement comply with the standard ASTM C150. Aggregate can be divided into two different categories: coarse aggregate and fine aggregate. Figure 7 shows the coarse (a) and fine (b) aggregates used in this study. Coarse aggregates are larger

particles that retain on a #4 sieve and are usually larger than 4.75 mm. The maximum coarse aggregate used in this study is ¾ in. and consists of round and fractured round particles. Fine aggregates are smaller particles, usually sand or crushed stone. The fine aggregate used in this work is a general concrete sand, a mix of both coarse and fine sands. The aggregates meet the requirements of the ASTM C33/C33M standard. The coarse and fine aggregates used in this study are from Bozeman Brick Block & Tile in Bozeman, Montana.

Figure 7. (a) Coarse aggregate, (b) Fine aggregate.

The volume of entrained air typically varies between 2% - 8% of the total volume of the concrete. In this study, AE 200 air entrainment from BASF is used, and the dosage was 0.75 ounce per 100 lb of cementitious material. Water is a key component in a concrete mix, causing hydration to occur when mixed with cement. Simply tap water was used in the mixes.

Rebar

Rebar is used in concrete construction to improve the tensile strength of the concrete members. The most common type of rebar is steel, because it is readily available and because is has a similar coefficient of thermal expansion as concrete. In this study, Grade 60 (yield strength of 60 ksi) conventional steel rebars are used. Two #3 rebars (diameter = 0.375 in.) are provided in the compression zone of each beam and two #4 (diameter = 0.5 in.) rebars are provided in the tension zone. For stirrups, #2 rebar (diameter = 0.25 in.) is used. Figure 8 shows the rebars used in this work.

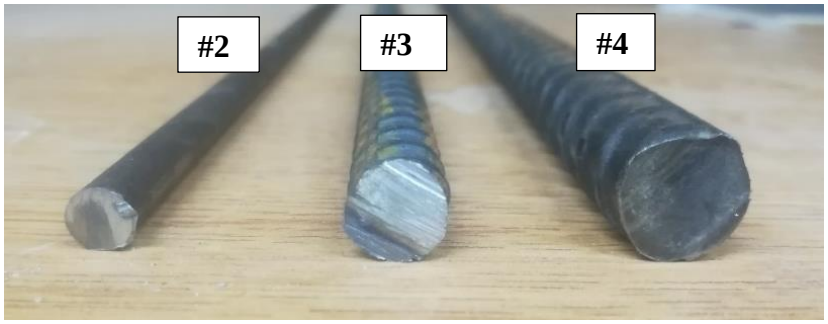

Figure 8. Rebar used in this study.

FRP Materials

Fiber Reinforced Polymer (FRP) wrapping is used in this work as a strengthening material. FRP is a composite material consisting of a fiber (e.g., glass, carbon, aramid, basalt, etc.) and polymer (e.g., epoxies, vinyl esters, polyurethanes, phenolics, etc.). One of the most common compositions of fiber is woven fabrics. FRP composites are anisotropic, with the best mechanical properties in the direction of the fibers. The main reasons behind using FRP as a strengthening and construction material are its high strength to weight ratio, resistance to corrosion, low production

and installation time, and easy maintenance. Despite having these advantages, FRP also has some drawbacks, including risk of fire, high initial cost, and requirement of a skilled worker.

Fiber Fabrics

In this work, two types of fiber fabrics are used, carbon and glass (see Figure 9). The fabrics are manufactured by US Composites, located in West Palm Beach, Florida. Both the carbon and glass fiber fabrics are 4 inches in width. Other properties of the fabrics are shown in Table 7.

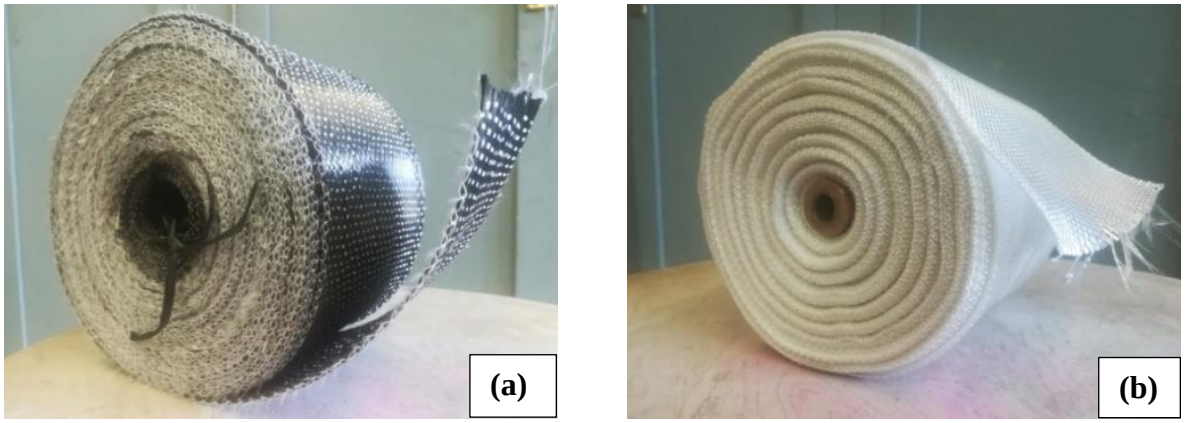

Figure 9. (a) Carbon fiber fabric, (b) Glass fiber fabric.

Table 7. Fiber properties (data provided by manufacturer, US Composites).

FRP type	Thickness (inch)	Weave	Weight (oz/yard^2)
Carbon fiber	0.021	Unidirectional	8.7
Glass fiber	0.011	Plain	11.0

Epoxy Resin

A high-strength epoxy used in this research, cured at room temperature, and had a medium viscosity. The product is System 2000 Laminating Epoxy Resin, manufactured by FibreGlast. A high-performance hardener with a pot life of 20 minutes was used with this resin system: 2020 Hardener. Other specifications of the epoxy resin from FibreGlast are shown in Table 8.

Table 8. Product specifications of epoxy resin (data provided by manufacturer, FibreGlast).

Color	Amber
Viscosity, @ 77°F	150-175 cps
Specific gravity	0.96 gms. /cc
Mix Ratio, by weight (resin : hardener)	100 : 23
Mix Ratio, by volume (resin : hardener)	4 : 1
Hardener pot life	20 minutes

Thermocouple

Type T thermocouple is used throughout this experimental work, cast in the concrete, to measure the temperatures in different conditions and at various locations in the beams. This type of thermocouple is suitable for measuring low temperature. It consists of a Copper wire (+) and Constantan (Cu and Cu-Ni) alloy wire (-). A type T thermocouple is shown in Figure 10, where the blue and red wires are Copper and Constantan, respectively.

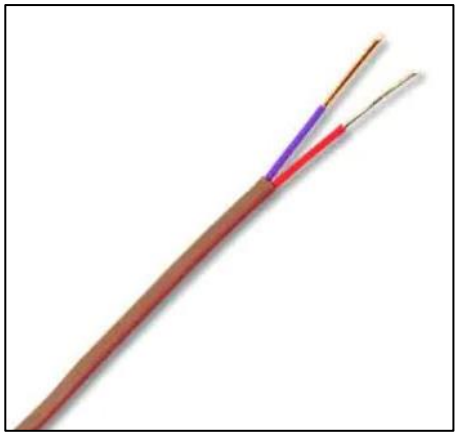

Figure 10. Type T thermocouple (Omega Engineering Inc.).

CHAPTER FOUR

MATERIAL TESTS

Introduction

This chapter discusses the test procedures, experimental setups, and material property results of the concrete and FRP materials used in this study. The preparation of the different test specimens, such as concrete cylinders and FRP coupons, are also discussed in this chapter.

Concrete

Specimen Preparation

A total of seven batches of concrete were cast for the seven beams in this study – six test series beams and one additional beam used for determining the thermal properties of the concrete (discussed in Appendix C). For each batch, nine cylinders were made to perform compressive strength tests at 7, 28 and 35 days (three cylinders per test day). The construction of the cylinders followed ASTM C31/C31M − 19a. Standard plastic cylinder molds (4 in. diameter, 8 in. height) were used for casting and a 3/8” diameter steel rod was used for tamping. After initial setting for around 24 hours, the molds were removed (Figure 11a) and the concrete cylinders were placed in a temperature-controlled 100% humidity cure room (Figure 11b) until the test day. The only exceptions are the cylinders tested at -40° C, which were placed in the cold room for around 24 hours after 34 days initial curing. The frozen cylinders were tested on day 35, the same day as beam testing.

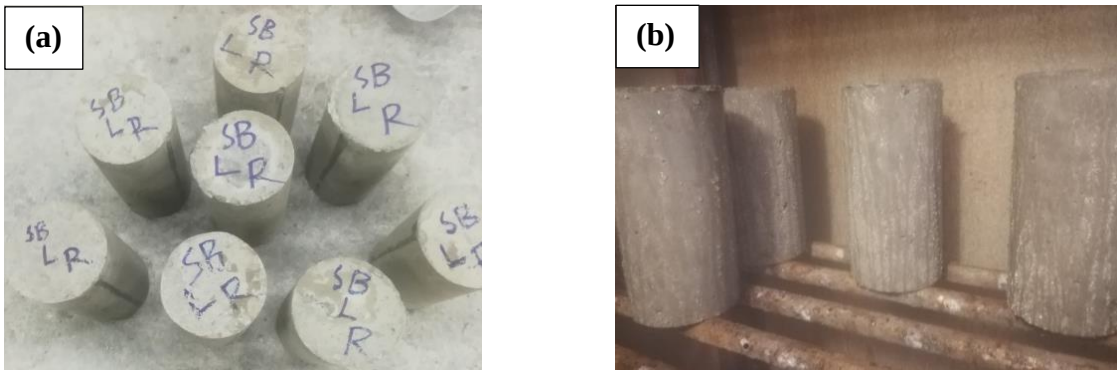

Figure 11. Example Cylinders; (a) Directly after mold removal, (b) In cure room.

Test Setup and Instrumentation

The compressive strength tests of the concrete cylinders were performed following the ASTM C39/C39M standard. The moisture on the surface of the cylinders was removed after removing them from the moist room. Two neoprene caps were placed on the top and bottom of the cylinders before testing. The tests were performed using the MTS Criterion C64 machine located in the Materials Testing Lab, MSU. The test setup for the concrete compressive strength tests is shown in Figure 12 (a) and Figure 12 (b) shows an example cylinder after testing.

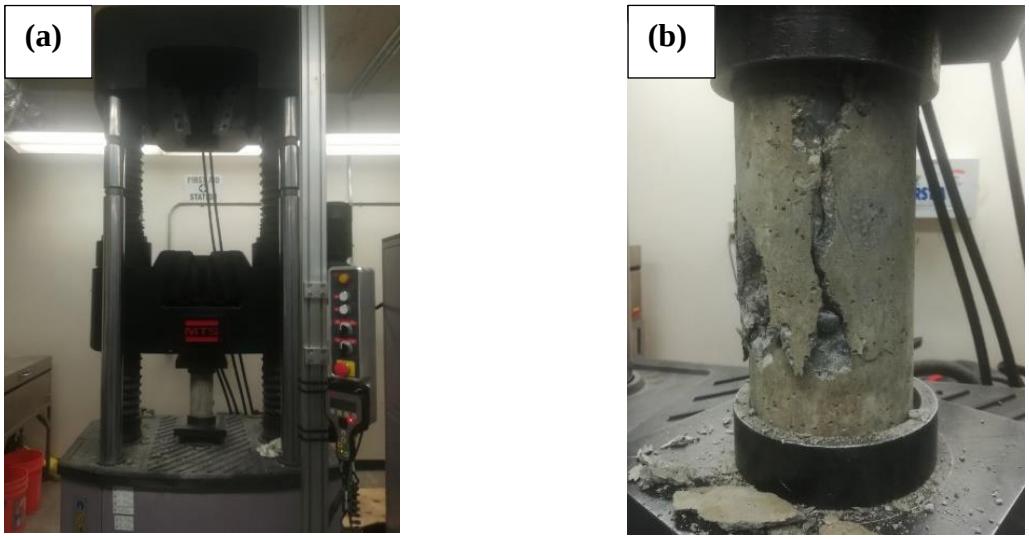

Figure 12. (a) Experimental setup of compression strength tests of concrete cylinders, (b) Example cylinder after test.

Results

Nine concrete cylinders were cast for each batch of concrete. Compression strength tests (ASTM C39/C39M) were performed for 7, 28 and 35 days (three cylinders each test day). Testing on day 35 was added to establish the concrete strength on beam test days. The strengths from the three specimens for each test day were averaged, with the exception of any outliers, and the average value was used to calculate the corresponding beam capacity. Slump tests (ASTM C143 / C143M) were also performed for each batch and those results along with the average concrete compressive strengths are shown in Table 9. Compressive strengths vs. ages of the concrete for each beam are plotted in Figure 13 (only including the room temperature cure room cylinder compressive strengths). Note, the beam acronyms listed in Table 9 and Figure 13 will be explained in detail in Chapter 5 of this thesis.

Table 9. Results summary of concrete cylinder testing.

Beam acronym	**Slump value**	**Day**	**Average concrete strength (ksi)**
CBRT	1”	7	4.14
		28	5.79
		Test day (35)	5.99
CBCT	5”	7	3.24
		28	4.36
		Test day (35)	4.36
SBLRT	2”	7	4.27
		28	5.58
		Test day (35)	5.53
SBLCT	2”	7	4.31
		28	5.72
		Test day (35)	6.15
SBLTRT	3”	7	3.47
		28	4.33
		Test day (35)	5.14
SBLTCT	1.5”	7	4.14
		28	4.71
		Test day (35)	5.61

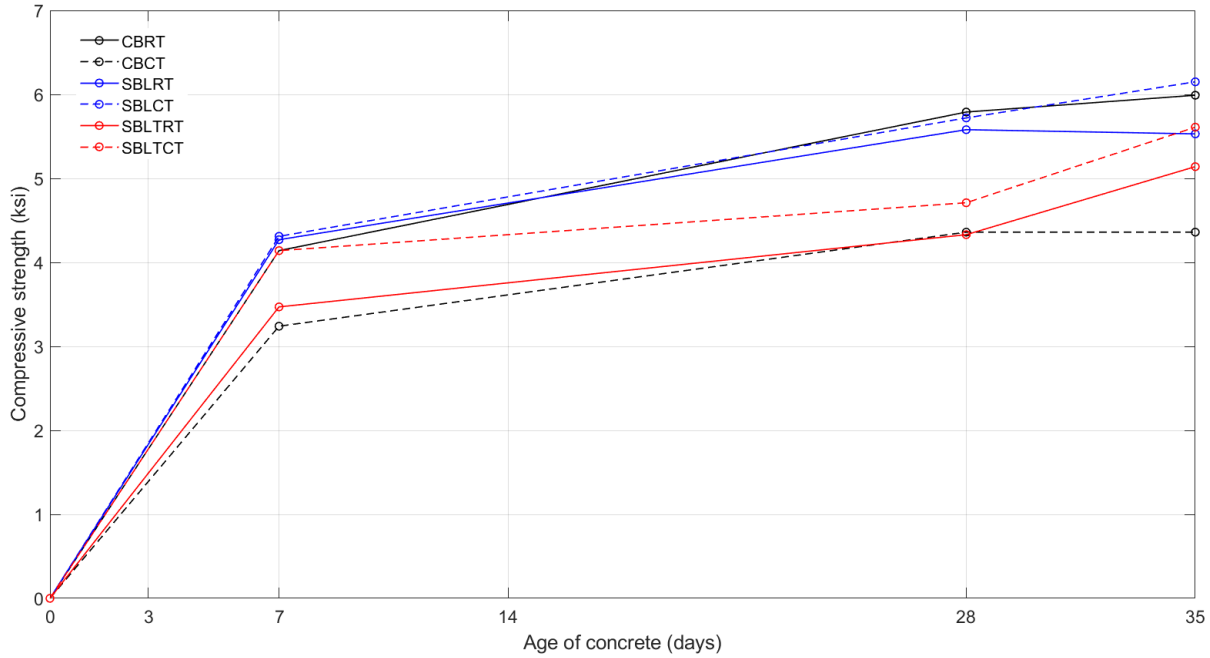

Figure 13. Compressive strength vs. age of concrete.

The strength of concrete is affected when it freezes and is held at low temperatures. To evaluate the effects that temperature had on the concrete strength in the cold room beams, four cylinders were kept in the cold room (-40^{o}C) for 24 hours (after being fully cured in the cure room for 34 days) and then tested for compressive strength. Table 10 shows the comparison between the concrete strength of the frozen cylinders (kept in cold lab for 24 hours after initial curing) and the cylinders tested at room temperature. For the same batch of concrete, on average the frozen cylinders had concrete strengths 87.18% higher than the room temperature concrete.

Table 10. Comparison between average concrete strengths at cold and room temperatures.

Specimen	**Average concrete strength at room temperature (ksi)**	**Concrete strength at cold temperature (ksi)**	**Percent increase (%)**
1 (SBLCT)	6.15	10.73	74.47
2 (SBLRT)	5.33	11.46	115.00
3 (SBLTCT)	5.61	8.86	57.93
4 (SBLTRT)	5.14	10.35	101.36

Fiber Reinforced Polymers

Specimen Preparation

Two sets of FRP coupons (CFRP and GFRP) were made to undergo tensile strength testing to determine the required material properties for hand calculations. In each set there were three specimens. The epoxy resin was applied to each specimen and then left to dry and cure for 2 days. The specimens were then cut in size and the dog bone tab, made of fiber glass plate, was attached. Figure 14 shows a schematic diagram of the FRP coupons with dimensions labeled and Table 11 lists the dimension details. A 125Ω resistance strain gauge (1.5 mm × 3 mm) was attached to one of the coupons in each set to allow the load-displacement data to be recorded, while the others were simply tested for maximum capacity. Figure 15 shows the coupons tested in this work.

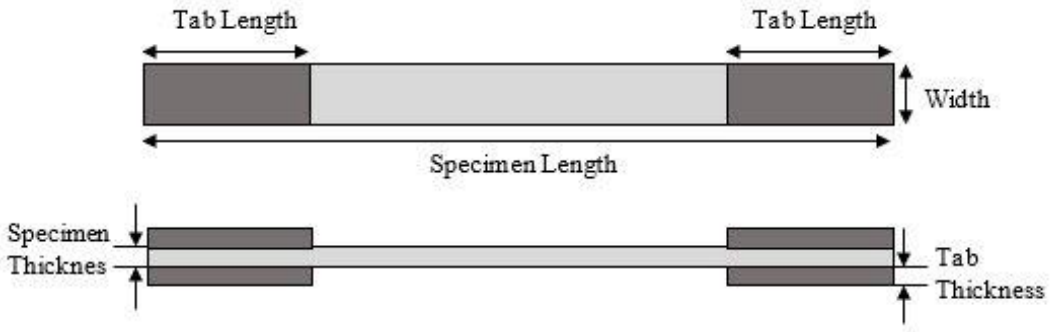

Figure 14. Schematic diagram of FRP coupons.

Table 11. Dimensions of FRP coupons.

FRP	coupon	Specimen width (inch)	Specimen thickness (inch)	Specimen length (inch)	Tab thickness (inch)	Tab length (inch)
CFRP	1	0.979	0.025	9	0.06	2.25
	2	0.977	0.031			
	3	0.979	0.026			
GFRP	1	0.981	0.018			
	2	0.975	0.020			
	3	0.978	0.019			

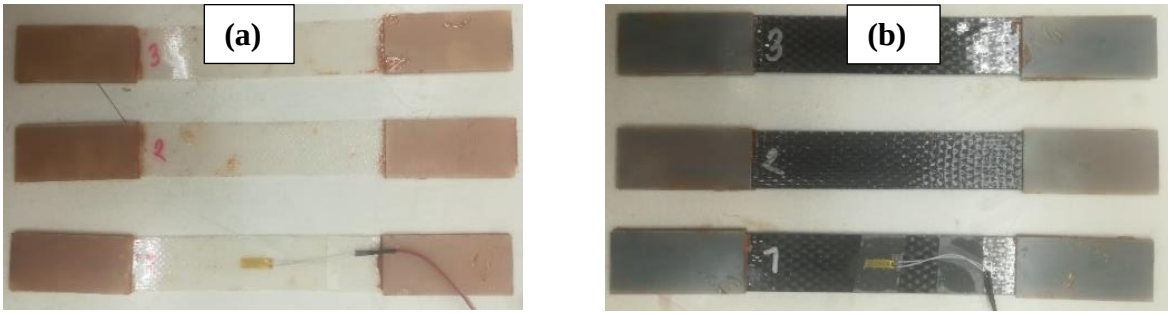

Figure 15. FRP coupons; (a) GFRP, (b) CFRP. The bottom specimen in each photograph is the one with the strain gauge attached.

Test Setup and Instrumentation

The tensile strength tests of the FRP coupons were performed following the ASTM d3039 standard. The tests were performed using the Universal Electromechanical Testing Machine located in the Composite Materials Lab, MSU. The loading rate was 0.001 in/sec. Figure 16 shows the test setup for the FRP coupons.

Figure 16. Experimental setup of FRP coupons; (a) Example coupon, (b) Zoomed in photograph of example coupon with strain gauge attached.

Results

The goal was to calculate the theoretical FRP strengthened beam capacity after gathering the modulus of elasticities from the experimental data. The ultimate load capacities of all coupons

were recorded and the load vs. displacement data was recorded for one of the coupons from each set. The data is summarized in Table 12 and the stress vs. strain plots (calculated from the load vs. displacement raw data), for both CFRP and GFRP are shown in Figure 17.

Table 12. Tensile strength test results of FRP coupons. Standard deviation values are shown in parentheses next the average values.

FRP	Coupon	Ultimate capacity (lbs)	Average ultimate capacity (lbs)	Yield strength (ksi)	Average Yield strength (ksi)	Modulus of elasticity (ksi)
CFRP	1	4808	4806 (22.10)	196.44	181.33 (20.56)	11.68E3
	2	4783		157.92		-
	3	4827		189.63		-
GFRP	1	534	524.67 (46.70)	30.24	28.26 (2.46)	1.94E3
	2	566		29.03		-
	3	474		25.51		-

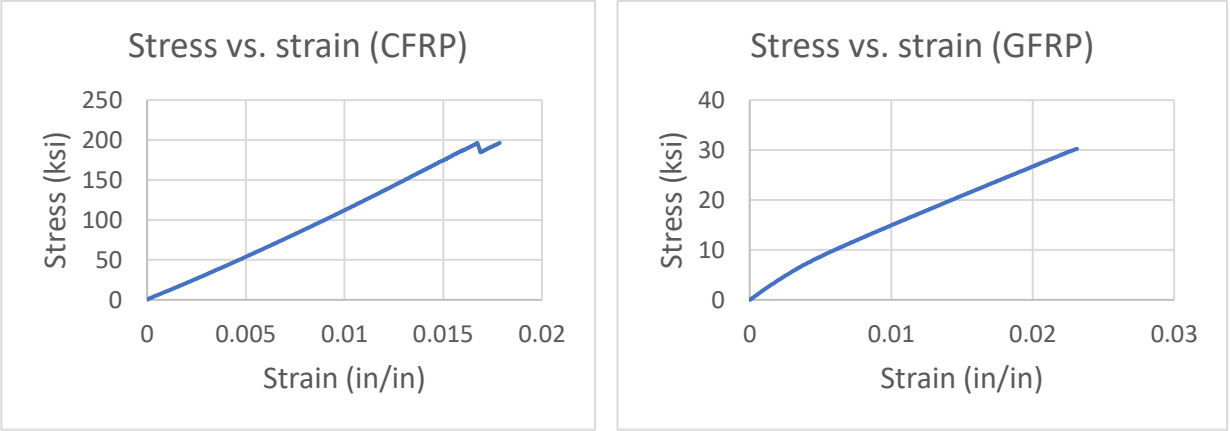

Figure 17. Stress-strain graphs of FRP; CFRP (left) and GFRP (right).

From the FRP coupon tensile strength test results, it can be observed that the CFRP used in this study has significantly higher yield strength and modulus of elasticity values than the GFRP (more than an order of magnitude), and this trend has been validated by other studies (Chawla 2011 and Tang 1997).

CHAPTER FIVE

BEAM TESTS

Introduction

This chapter presents the test matrix used in this research and discusses the construction of the beams in this study. Additionally, the beam test setup at both room and cold temperature conditions is explained. The experimental results, including ultimate capacities, stiffnesses, and FRP failure mechanisms, of the control and strengthened beams at both temperature conditions are presented and discussed. The predicted ultimate flexural beam capacities of both control and strengthened beams are calculated following ACI standards and are compared with the experimental results.

Experimental Design

Two sets of beams (one for each temperature condition) were constructed for this study. In each set, there was one control beam and two strengthened beams. One of the strengthened beams was reinforced with CFRP in only the longitudinal direction, whereas the other strengthened beam was reinforced longitudinally with CFRP and transversely with GFRP. Beam cases and strengthening schemes are presented in Table 13. The acronyms assigned to each beam will be used throughout this chapter. The first two letters signify either control beam (CB) or strengthened beam (SB), the letters after SB signify either longitudinal (L) or longitudinal + transverse (LT), and the last two letters signify either room temperature (RT) or cold temperature (CT) testing conditions.

Table 13. Beam cases and strengthening schemes.

Beam acronym	**Case**	**No. of longitudinal wrapping with CFRP**	**No. of transverse wrapping with GFRP**	**Testing temperature condition**
CBRT	**C**ontrol **B**eam tested at **R**oom **T**emperature	-	-	Room temp.
SBLRT	**S**trengthened **B**eam with **L**ongitudinal wrapping tested at **R**oom **T**emperature	1	-	Room temp.
SBLTRT	**S**trengthened **B**eam with **L**ongitudinal + **T**ransverse wrapping tested at **R**oom **T**emperature	1	14 @ 4" edge to edge	Room temp.
CBCT	**C**ontrol **B**eam tested at **C**old **T**emperature	-	-	-40^0C
SBLCT	**S**trengthened **B**eam with **L**ongitudinal wrapping tested at **C**old **T**emperature	1	-	-40^0C
SBLTCT	**S**trengthened **B**eam with **L**ongitudinal + **T**ransverse wrapping tested at **C**old **T**emperature	1	14 @ 4" edge to edge	-40^0C

For each beam, a batch of concrete was made following the mix shown in Table 6. All six beams were identical when initially cast, with the same steel reinforcement and overall dimensions. Figures 18 and 19 show the elevation and cross-section, respectively, of the beams, including reinforcement details. The beams had a 6 in. × 8 in. cross-section and a span length of 108 in. In the longitudinal direction, two #3 (diameter = 0.375 in.) rebars were placed symmetrically in the compression zone, and two #4 (diameter = 0.5 in.) rebars were placed symmetrically in the tension zone. The stirrups consisted of #2 rebars at 4 in. c/c., except for a 10 in. gap at center span.

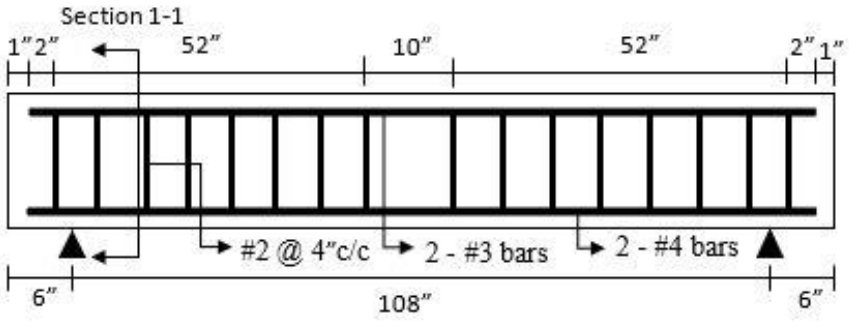

Figure 18. Beam elevation.

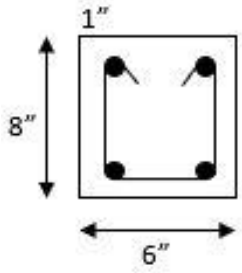

Figure 19. Beam cross section (Section 1-1 shown in Figure 18).

Two type T thermocouples were provided at the edge and at the middle of the cold room beams for taking temperature data. Figure 20 illustrates the position of the thermocouples in the beams.

Figure 20. Thermocouple; (a) At the edge, (b) At the middle.

For the longitudinal FRP strengthened beams, one layer of Carbon Fiber Reinforced Polymer (CFRP) was provided on the tension side of the RC beams by the wet layup method to increase the flexural strength. The 108 in. long CFRP layer had a width of 4 in. The longitudinal + transverse FRP beams consisted of the same longitudinal CFRP strengthening, with the addition of transverse GFRP wrapping @ 4 in. edge to edge. Figure 21 shows a schematic of the strengthened beams. Figure 21 (a) shows the tension side (bottom) of the longitudinal strengthened beams, and the other two figures show the longitudinal + transverse strengthened beams, with the Figure 21 (b) showing the bottom view and the Figure 21 (c) showing the sides.

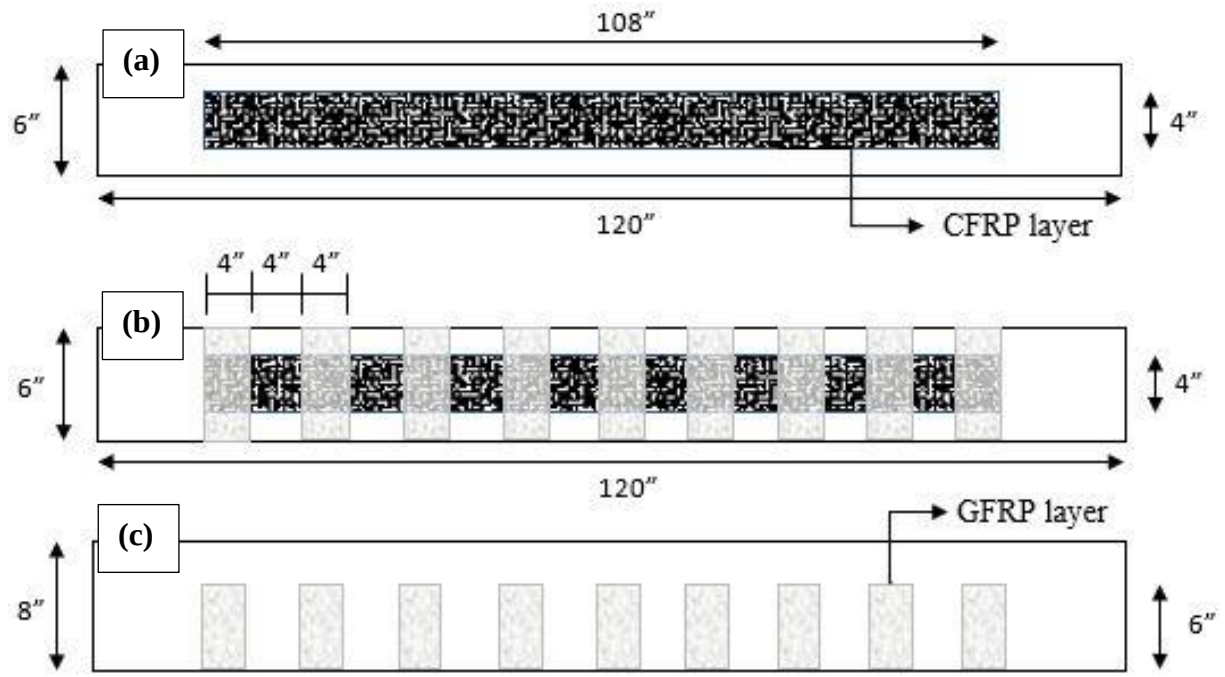

Figure 21. Strengthened beams; (a) Longitudinal, (b) Longitudinal + transverse (bottom view), (c) Longitudinal + transverse (side view)

The transverse wrapping is not expected to directly affect the longitudinal capacity of the beams but was included to enhance the bond between the CFRP longitudinal wrapping and the concrete.

The wet-layup installation method included the following steps (El-Gamal et al. 2015, Fafach et al. 2005):

a) Clean the surface of the concrete.

b) Apply epoxy to the concrete surface using a roller.

c) Place FRP sheet on structure.

d) Apply epoxy to sheet surface.

e) Finish and let the epoxy dry.

Figure 22 shows the application of the FRP to the beams, with (a) the epoxy resin application to the concrete surface and (b) placement of the FRP sheet to the concrete and epoxy resin application to the FRP surface.

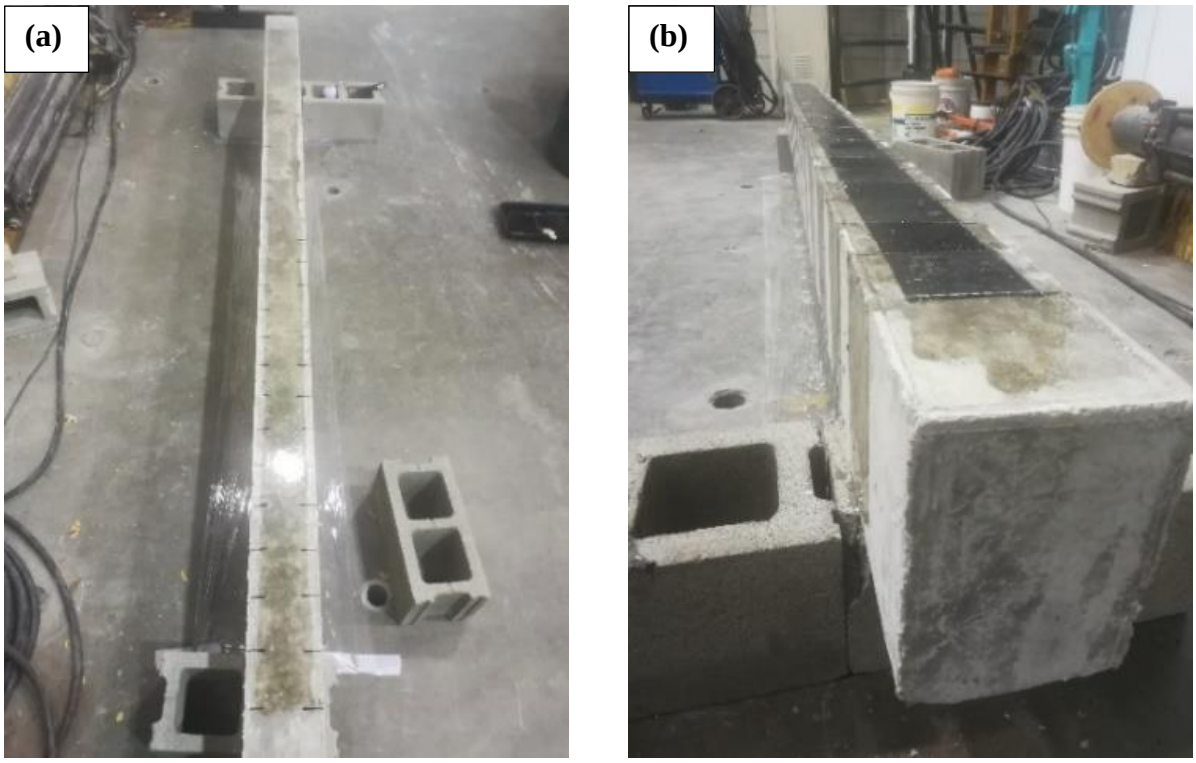

Figure 22. (a) Applying epoxy to the concrete surface, (b) Placing FRP sheet to the concrete and applying epoxy to sheet surface.

Figures 23 (a) and (b) show the longitudinal strengthened beams and the longitudinal + transverse strengthened beams, respectively, after FRP application. Note the beams are “upside down” in these photographs, opposite of beam testing orientation, allowing for application of the FRP.

Figure 23. (a) Longitudinal strengthened beams, (b) Longitudinal + transverse strengthened beams.

Figure 24 is a workflow chart, clearly showing the process followed for this research, including beam construction, curing, application of FRP and durations of different steps/processes. Some key points from Figure 24 are:

- Formwork was removed after 24 hours for all specimens.
- The beams were cured (in standard concrete curing conditions) for 28 days.
- After one day of removing beams from the cure room (allowing time for the concrete to dry), the FRP was applied and then left to dry and cure for 2 additional days.
- The cold beams were kept in the cold lab for 3 days prior to testing.
- All beams were tested on the 35^{th} day after being cast.

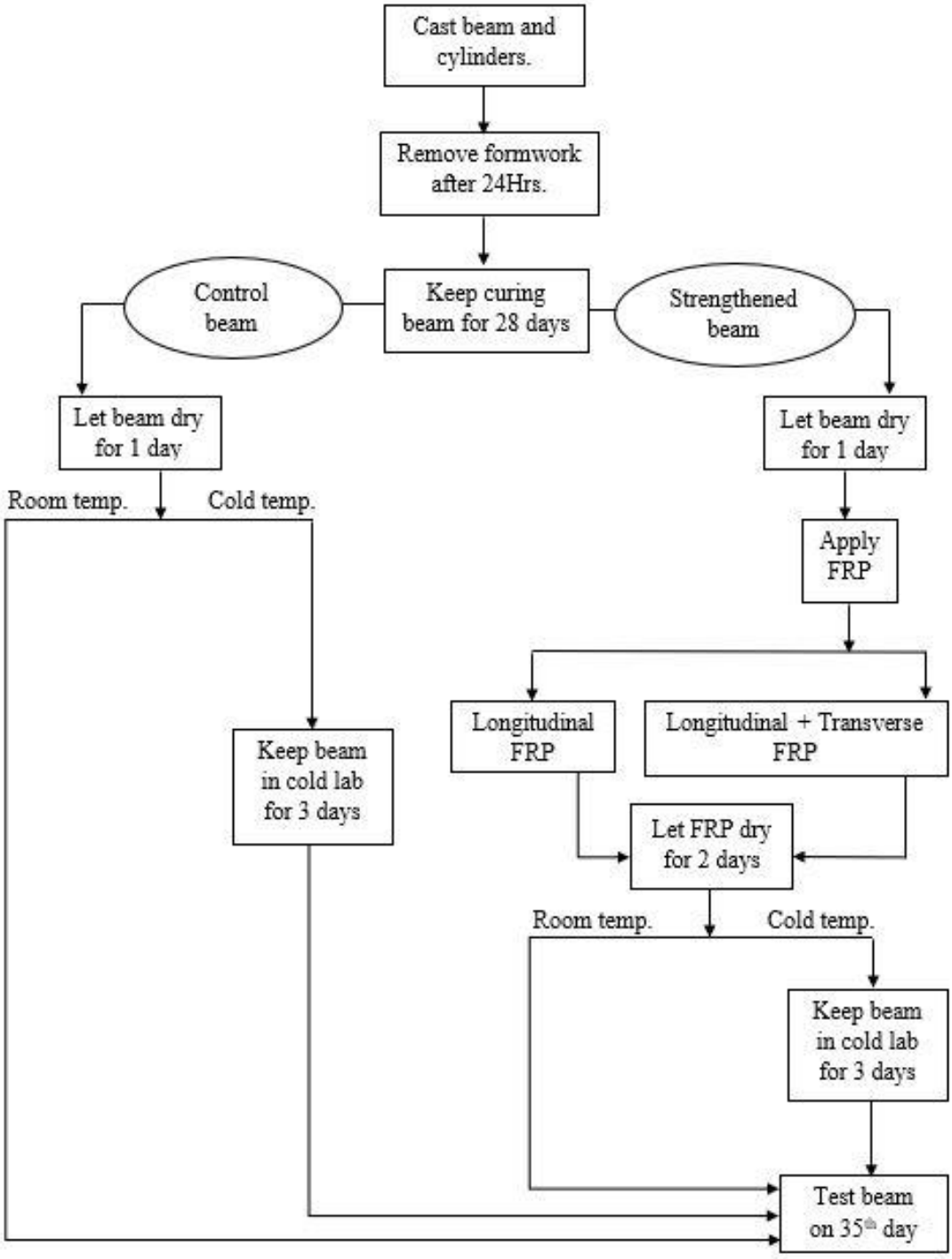

Figure 24. Workflow chart of the steps followed for this research.

Test Setup and Instrumentation

All beams were tested under four-point bending with the test setup is shown in Figure 25. Figure 26 shows the test setup for an example beam test at room temperature (a) and in the cold room (b). Two-point loads were applied at midspan, spaced at 18 in. between loads. This loading condition creates zero shear and constant moment in the center span of the beams. The test setup includes a rigid load frame, a load cell, and one load transfer element. The load was applied using a single hydraulic ram, and the beam behavior was monitored until failure. A strain potentiometer sensor was attached at exactly the midspan of the beam to collect deflection data. The load-deflection data was recorded by a data acquisition program written in LabView.

The thermal behavior of the concrete beams was studied in this research (Appendix B), and the results of this study led to the decision that the cold temperature test series beams should be tested in the cold room (as opposed to being brought out from the cold room to the room temperature test setup for testing). For the cold room tests, a heating cable was wrapped around the hydraulic ram cable that was connected to the load cell so that the hydraulic fluid stayed at the appropriate temperature and did not lose its viscosity during testing.

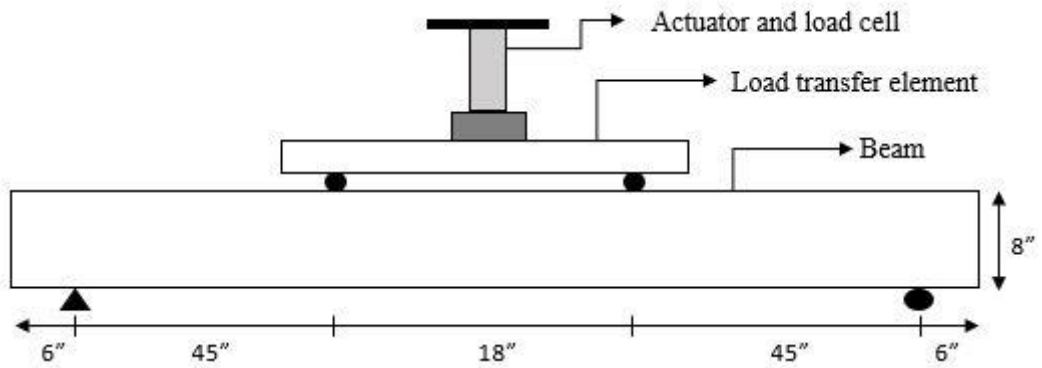

Figure 25. Schematic diagram of the beam test setup.

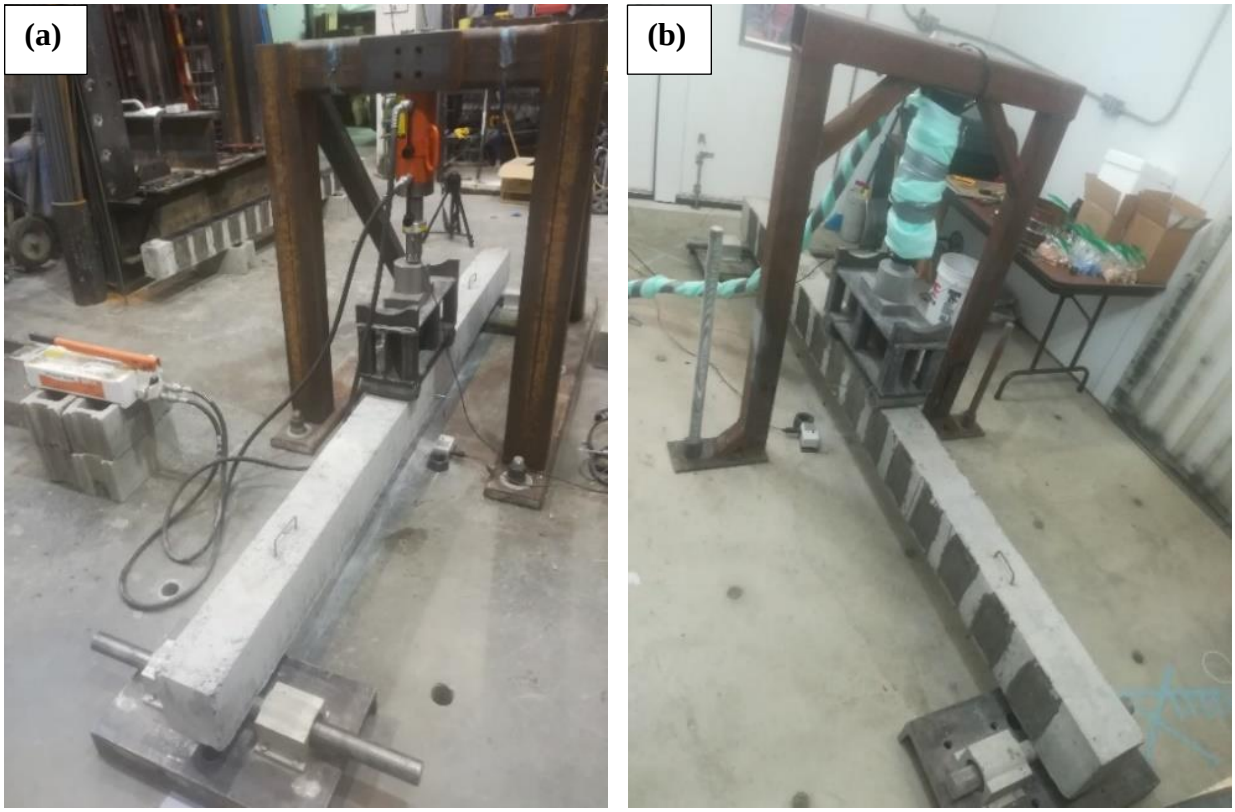

Figure 26. Test setup of example beams; (a) In room temperature, (b) In cold room.

The temperatures of the cold room beams before and after testing were measured using the thermocouple wires (previously shown in Figure 20) and the results are shown in Table 14. It can be seen that the temperatures remained fairly constant with an average of about -31.5ºC throughout testing.

Table 14. Temperature data of cold room beams.

Beam	**Beam temperature (ºC)**			
	Before testing		**After testing**	
	Middle	Edge	Middle	Edge
CBCT	-33.58	-31.34	-30.98	-28.98
SBLCT	-34.65	-31.95	-31.44	-30.34
SBLTCT	-32.66	-30.85	-31.54	-29.70

Predicted Capacities

The flexural capacity of the control RC beam was calculated following the ACI standards described in Appendix A of this thesis. As previously discussed, the transverse wrapping is not expected to directly affect the longitudinal capacity of the strengthened beams, and the capacity of the beams strengthened with longitudinal FRP was calculated per the detailed steps in Appendix A. It should also be noted that these calculations used the measured room-temperature compressive strengths for each beam (also included in this table). Cracking moments of the beams were also calculated. A summary of the predicted capacities for each beam are shown in Table 15.

Table 15. Summary of hand calculation results.

Beam	**Predicted beam capacity (kip) for f'_c = 4000 psi**	**Actual f'_c (psi)**	**Predicted beam capacity (kip) for actual f'_c**	**Cracking moment, M_{cr} (kip-ft)**	**Load (kip) required for M_{cr}**
CBRT	7.29	5990	7.34	3.10	2.06
CBCT		4360	7.30	2.64	1.76
SBLRT	11.30	5530	11.58	2.97	1.98
SBLCT		6150	11.65	3.14	2.09
SBLTRT		5140	11.53	2.87	1.91
SBLTCT		5610	11.59	3.00	2.00

Data Normalization

Although the mix design was the same for all beams, the concrete compressive strength (f'_c) of each beam differs. To consistently compare results, all the beam results are normalized to the targeted concrete compressive strength of 4000 psi and the details are shown in Table 16. In summary, the loads of the experimental raw data points were adjusted slightly by the same percentage that the hand calculations changed after taking into account the difference in predicted

capacities when using the actual f'_c of the concrete batches instead of the design strength of 4000 psi.

Table 16. Normalization results.

Beam	Actual f'_c (psi)	Calculated beam capacity		%	% increase	Need to decrease by	Beam capacity from test results	
		For actual f'_c	For f'_c = 4000 psi				Original (kip)	Normalized (kip)
CBRT	5990	7.34	7.30	100.66	0.66	0.99	9.84	9.77
CBCT	4360	7.31	7.30	100.16	0.16	0.99	11.48	11.46
SBLRT	5530	11.58	11.30	102.47	2.47	0.98	10.48	10.22
SBLCT	6150	11.65	11.30	103.07	3.07	0.97	11.23	10.89
SBLTRT	5140	11.53	11.30	102.02	2.02	0.98	9.61	9.42
SBLTCT	5610	11.59	11.30	102.56	2.56	0.97	13.10	12.75

To see the effects of the data normalization, Figure 27 shows the original experimental results of load vs. midspan displacement on the left (a) and the normalized data on the right (b). From this figure, it can be seen that the original and normalized graphs follow the same trends, and the differences between them are minimal. It should be noted that this finding is consistent with the expected behavior of tension controlled concrete beams. In these beams, the capacity is dominated by the yield strength of the reinforcement and compressive strength has little effect. To simplify the comparisons, the remaining graphs presented in this thesis are plotted and discussed using the normalized data.

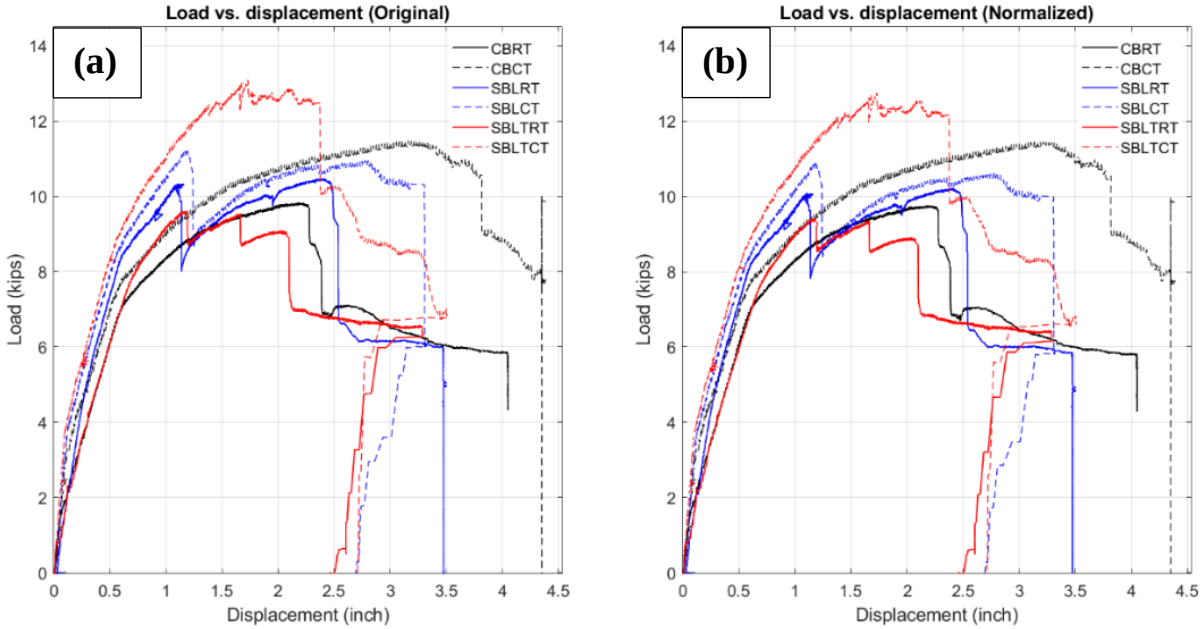

Figure 27. Load vs. displacement (at midspan) graph for all beams; (a) Original data, (b) Normalized data.

Experimental Results

Control Beams

The load vs. displacement graphs of the control beams at both room and cold temperatures are shown in Figure 28 (a) and (b), respectively. The plots depict that the first visible flexural cracks formed at around 1.87 kips and 2.47 kips for CBRT and CBCT, respectively. It was confirmed visually during testing and in video footage that these initial flexural cracks occurred in the constant moment region (center-span) of the beams. The ultimate loads taken by the CBRT and CBCT beams were 9.77 kips and 11.46 kips, respectively, and the displacements at these points were 2.18 in. and 3.16 in., respectively.

Beam stiffness is also shown in the plots (Figure 28), which is a chosen parameter to compare amongst all tested beams. For this research, the stiffnesses were calculated as the slopes of the normalized graphs. As a reminder, only the y-axis (load capacity) was normalized, and the

x-axis (displacement) is the original raw data from the experimental results. Calculation of stiffness from these graphs in this way may not quantitatively represent the exact beam stiffness, but since the same process was repeated for all beams, the results 1) give insight to an understanding of how the stiffness changes along the graph and 2) yield a measure to compare all of the different beams of this study. In the initial linear part of the graphs, the CBRT and CBCT beam stiffnesses were 22.6 k/in. and 29.6 k/in., respectively. Then as the loading increases, stiffness decreases for both beams.

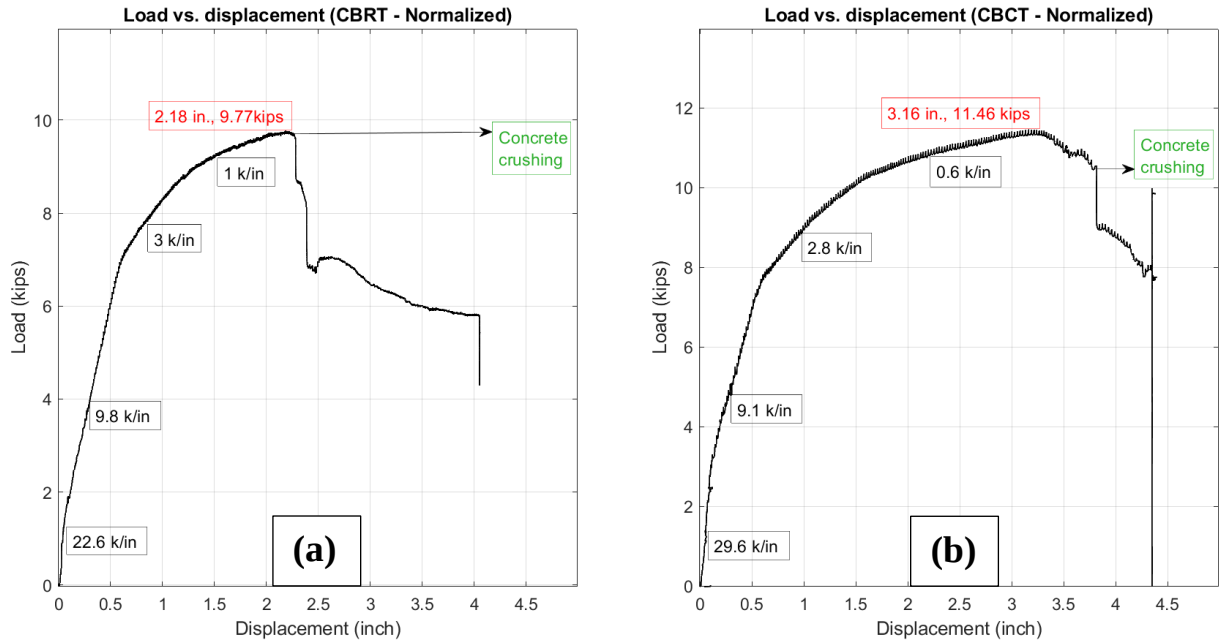

Figure 28. Load vs. displacement graph; (a) CBRT, (b) CBCT. Black boxes are stiffness labels and red boxes are ultimate capacity points. The point of concrete crushing is labeled in green.

The control beams at both temperature conditions failed very similarly. As predicted, the failure pattern followed the typical RC beam flexural failure. Figures 29 and 30 show photographs of the CBRT and CBCT beam failures, respectively, with (a) showing flexural cracks forming throughout testing (lines made thicker and darker for a better visual) and (b) showing the concrete

crushing at the end of testing. At first the flexural cracks were visible in the constant moment region and then continue along the beam as the load increased. Also, as the loads increased, the widths of the cracks increased. The load was applied until the concrete crushed and the beams lost load bearing capacity.

Figure 29. CBRT beam failure; (a) Flexural cracks forming throughout testing, (b) Concrete crushing at end of testing.

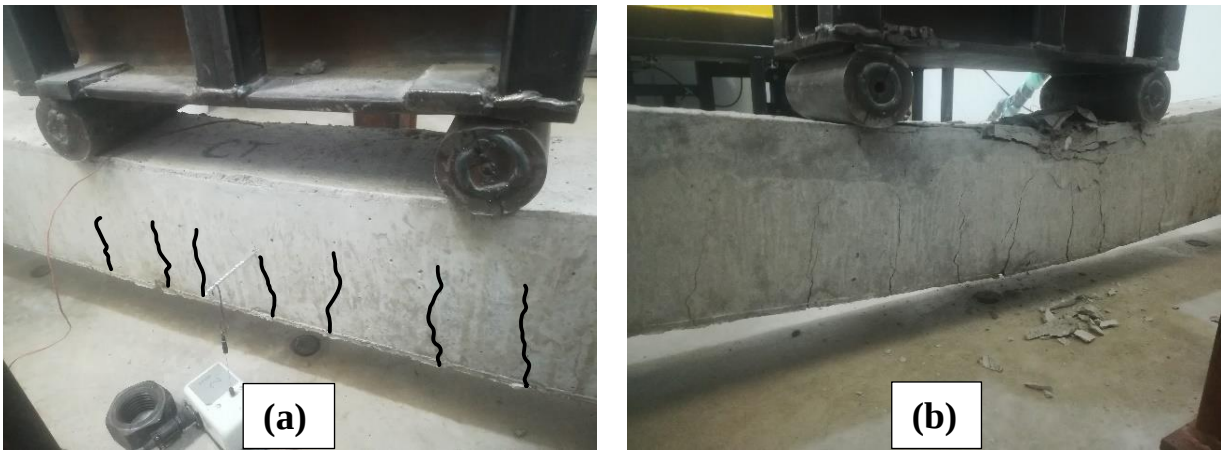

Figure 30. CBCT beam failure; (a) Flexural cracks forming throughout testing, (b) Concrete crushing at end of testing.

Longitudinal Strengthened Beams

Figure 31 shows the load vs. displacement graph of the longitudinal strengthened beams at both room temperature (a) and cold temperature (b). From the plots, it can be said that, initially, the SBLRT and SBLCT beams formed the first visible flexural cracks at 1.78 kips and 1.97 kips, respectively. The debonding of the longitudinal CFRP occurred for SBLRT and SBLCT beams at 10.09 kips and 10.89 kips, respectively, and displacements at these points were 1.11 in. and 1.20 in., respectively. After the delamination drop, the load then continues to increase and the post-delamination ultimate loads taken by the SBLRT and SBLCT beams were 10.22 kips and 10.62 kips, respectively, at the displacements of 2.41 in. and 2.78 in., respectively. Initially, the SBLRT and SBLCT beam stiffnesses were 23.4 k/in. and 32.7 k/in., respectively. Like the control beams, with higher loading, stiffness decreases for both beams.

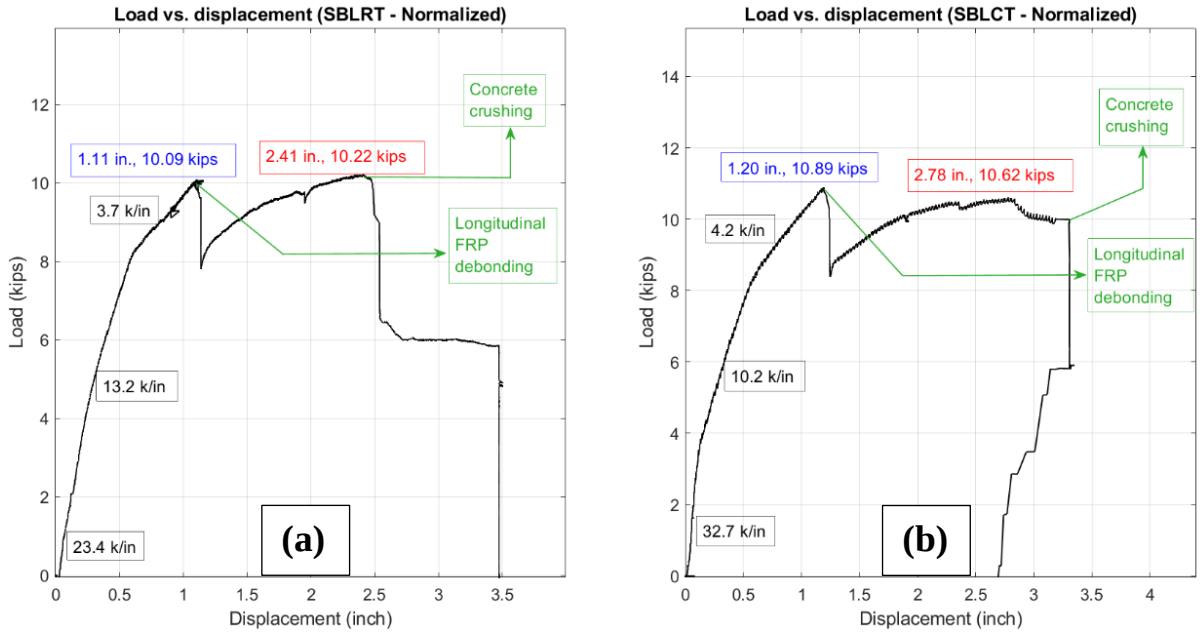

Figure 31. Load vs. displacement graph; (a) SBLRT, (b) SBLCT. Black boxes are stiffness labels, blue boxes are longitudinal FRP delamination points, and red boxes are post-delamination ultimate capacity points. The points of longitudinal FRP debonding and concrete crushing are labeled in green.

The photographs of the failure patterns for SBLRT and SBLCT are shown in Figures 32 and 33, respectively. Each of the figures includes pictures of (a) flexural cracks forming (again darkened to make more apparent), (b) debonding of longitudinal FRP, and (c) concrete crushing. At the initial stage of loading, the flexural cracks started forming, and the width of the cracks increased with higher loading. Both the beams were loaded until the compression concrete crushed.

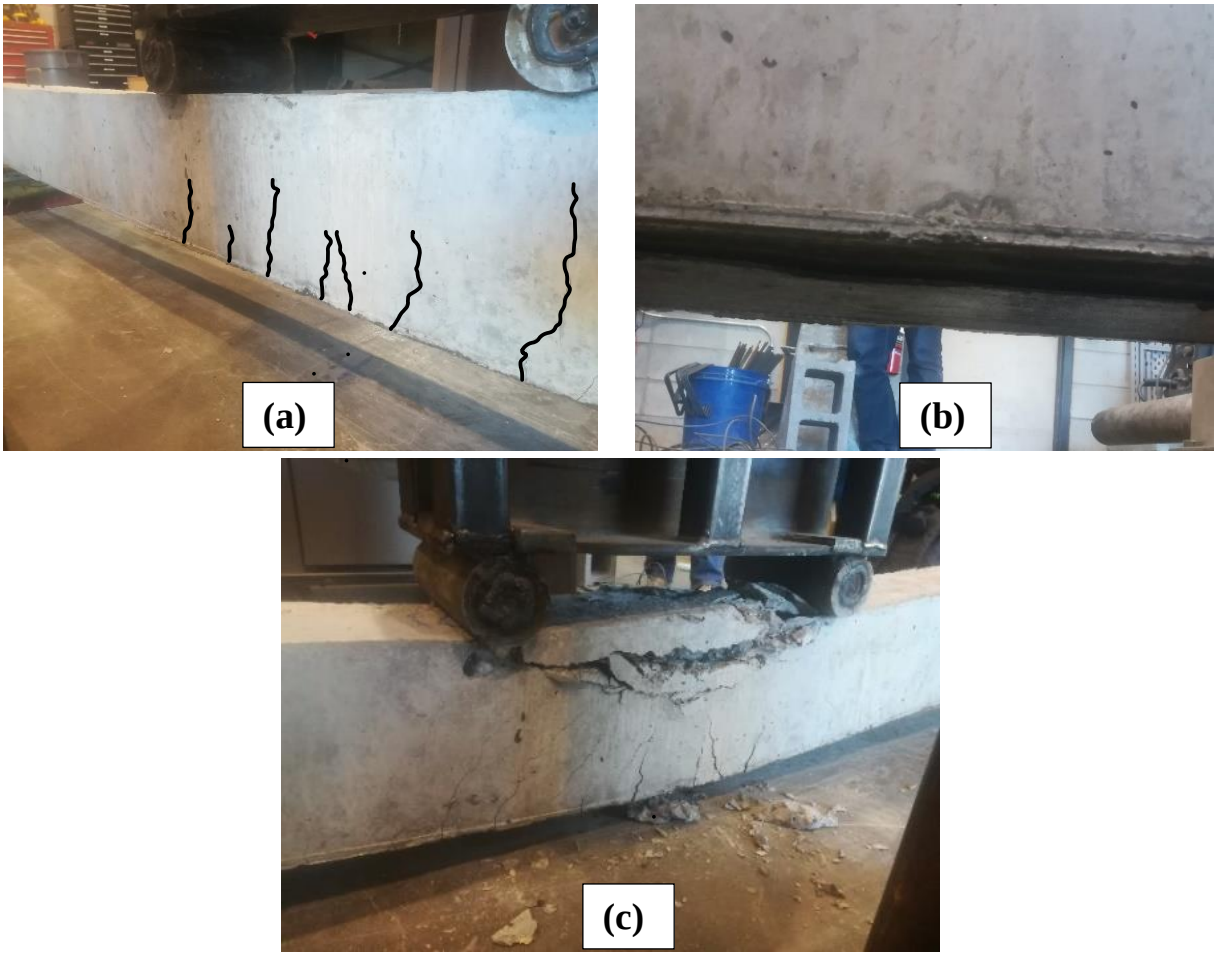

Figure 32. SBLRT beam failure; (a) Flexural cracks, (b) Debonding of longitudinal FRP, (c) Concrete crushing.

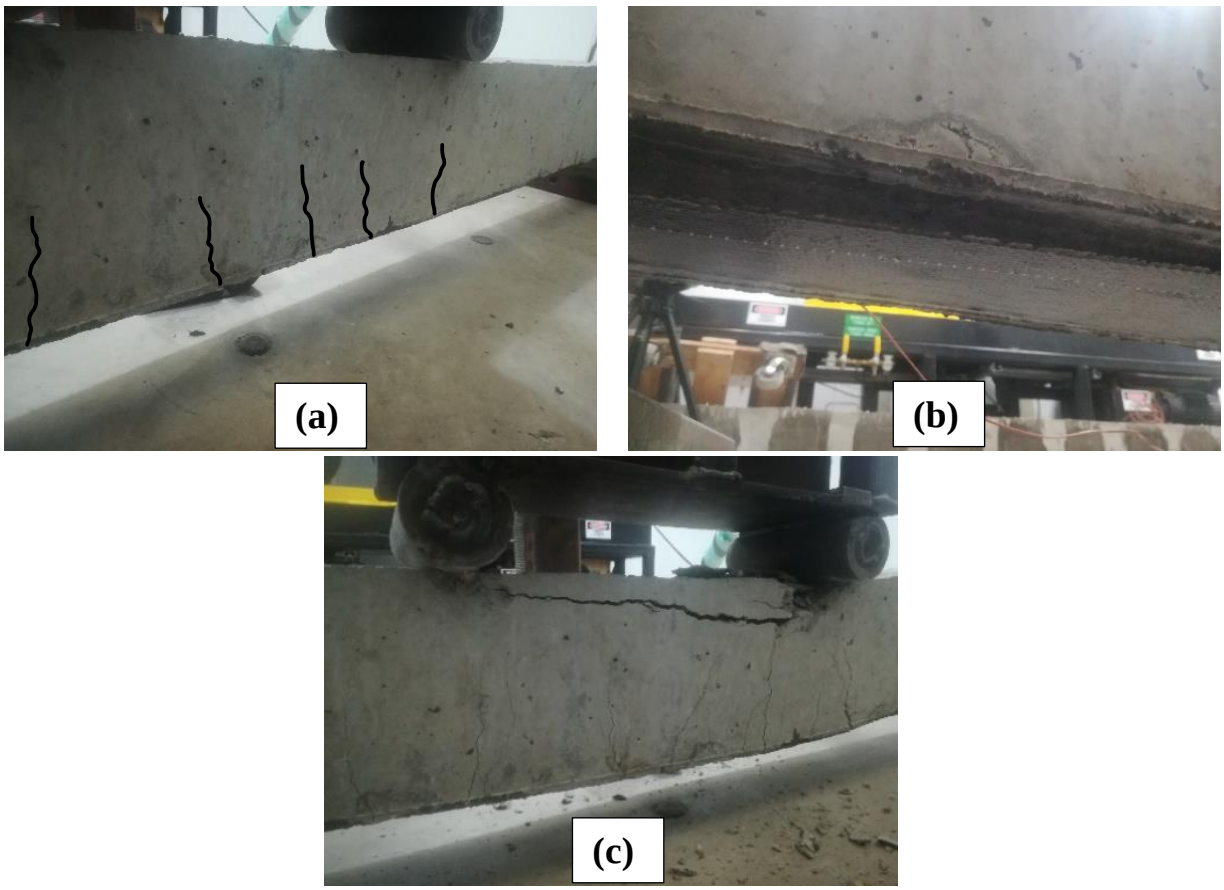

Figure 33. SBLCT beam failure; (a) Flexural cracks, (b) Debonding of longitudinal FRP, (c) concrete crushing.

Longitudinal + Transverse Strengthened Beams

The load vs. displacement graphs of the longitudinal + transverse strengthened beams at both room and cold temperatures are shown in Figure 34 (a) and (b), respectively. The plots depict that flexural cracks started becoming visible at around 0.85 kips and 1.96 kips for SBLTRT and SBLTCT, respectively, and again from the visual during testing and video footage, initial cracks occurred in the constant moment region (center-span). The longitudinal FRP delaminated at around 9.36 kips and 12.17 kips for SBLTRT and SBLTCT, respectively, and displacements at these points were 1.66 in. and 2.37 in., respectively. The ultimate loads carried by the SBLTRT and SBLTCT beams were 9.42 kips and 12.75 kips, respectively, where the displacements were 1.18

in. and 1.73 in., respectively. Conversely to what happened for SBLRT and SBLCT, the ultimate capacities of both longitudinal + transverse strengthened beams occurred before the longitudinal wrapping delaminated, and additionally, the concrete crushing failure occurred rather quickly after delamination as opposed to the reloading that occurred for the longitudinal only strengthened beams. Similar to the control and longitudinal strengthened beams, the stiffnesses of the longitudinal + transverse strengthened beams decrease with the increase in loading. Initially, the stiffnesses of SBLTRT and SBLTCT beams were 16 k/in. and 36.2 k/in., respectively.

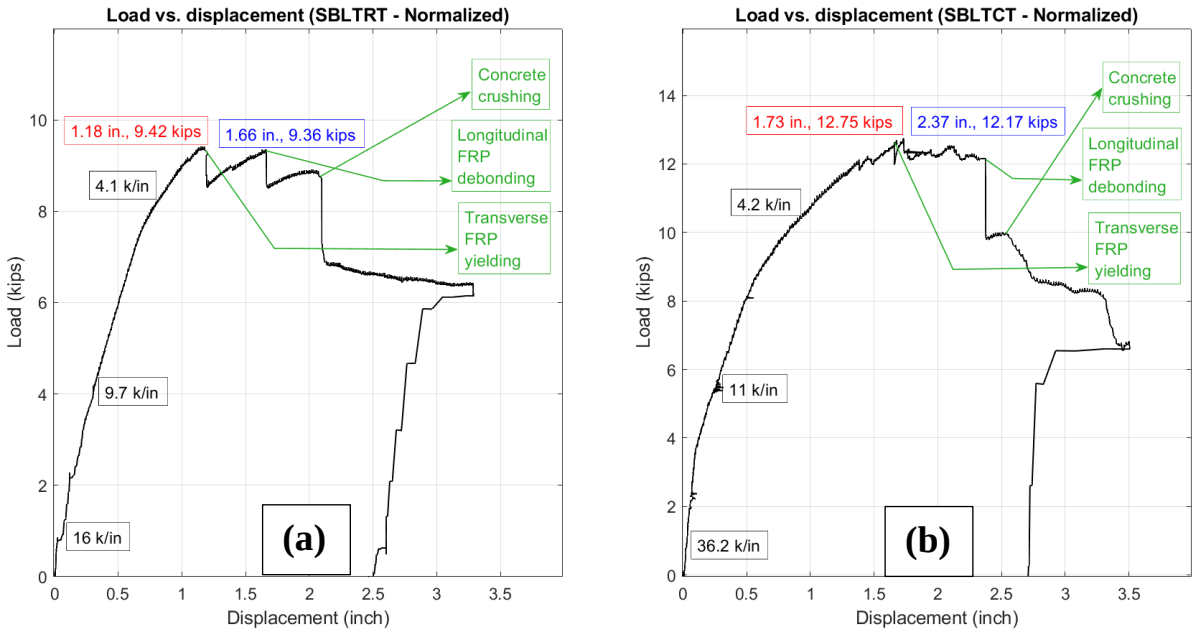

Figure 34. Load vs. displacement graph; (a) SBLTRT, (b) SBLTCT. Black boxes are stiffness labels, red boxes are ultimate capacity points, and blue boxes are longitudinal FRP delamination points. The points of transverse FRP yielding/delaminating, longitudinal FRP debonding, and concrete crushing are labeled in green.

The failure patterns of SBLTRT and SBLTCT beams were similar to each other and are shown in Figures 35 and 36, respectively. At initial loading, the flexural cracks started forming and becoming more visible with higher loading. The debonding of the longitudinal FRP was delayed due to the support from the transverse FRP. The widths of the flexural cracks increased,

and the transverse FRP started debonding from the concrete surface as the loads increased, shown by the red outlines in Figures 35 (b) and 36 (b). As the loading progressed, the transverse FRP tore at the bottoms of the beams (most clearly shown in Figure 36 (c)). After additional loading, the longitudinal FRP was delaminated and then the load continued to be applied until the concrete crushed.

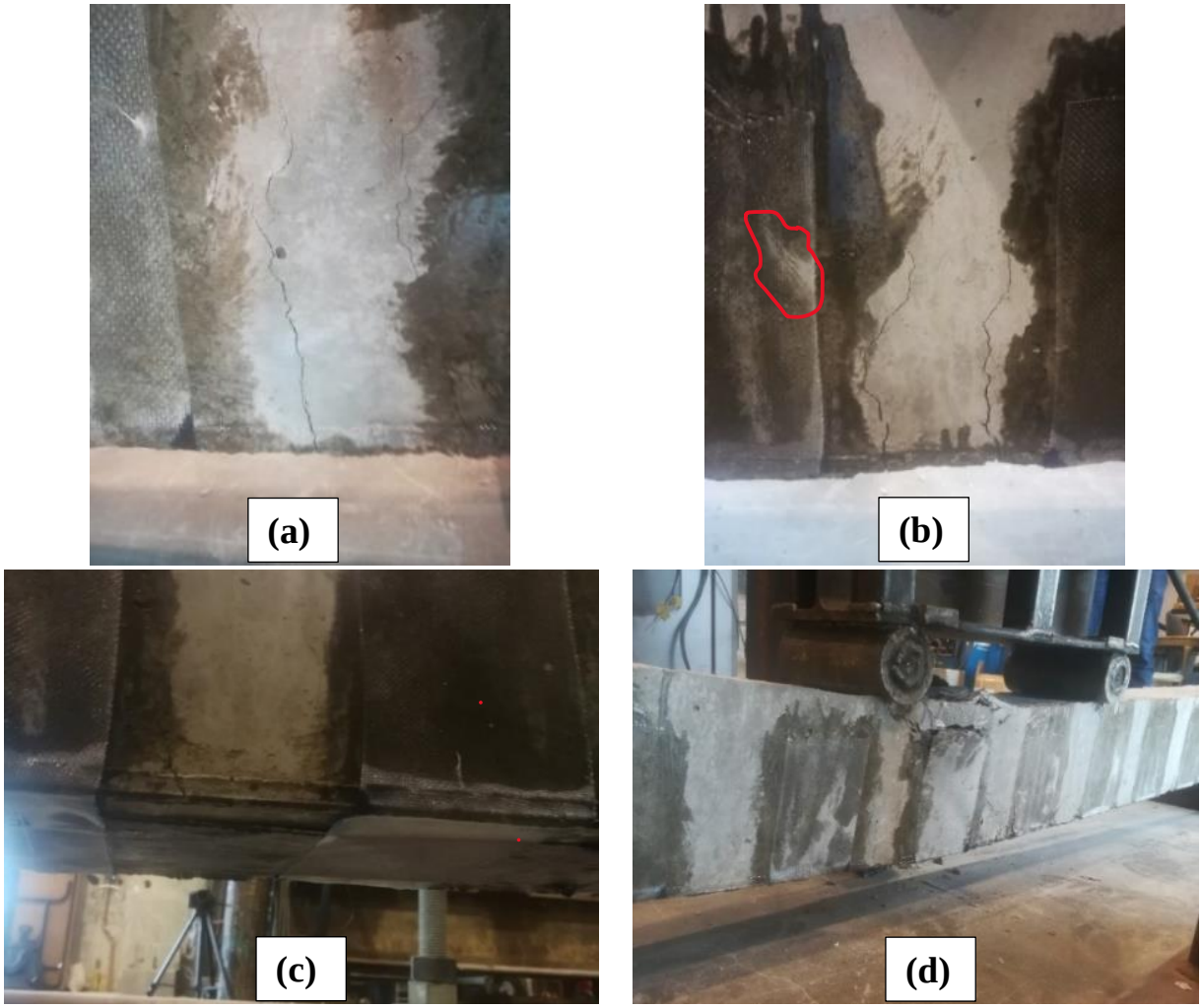

Figure 35. SBLTRT beam failure; (a) Flexural cracks, (b) Delamination of transverse FRP, (c) Debonding of longitudinal FRP and tearing of transverse FRP, (d) Concrete crushing.

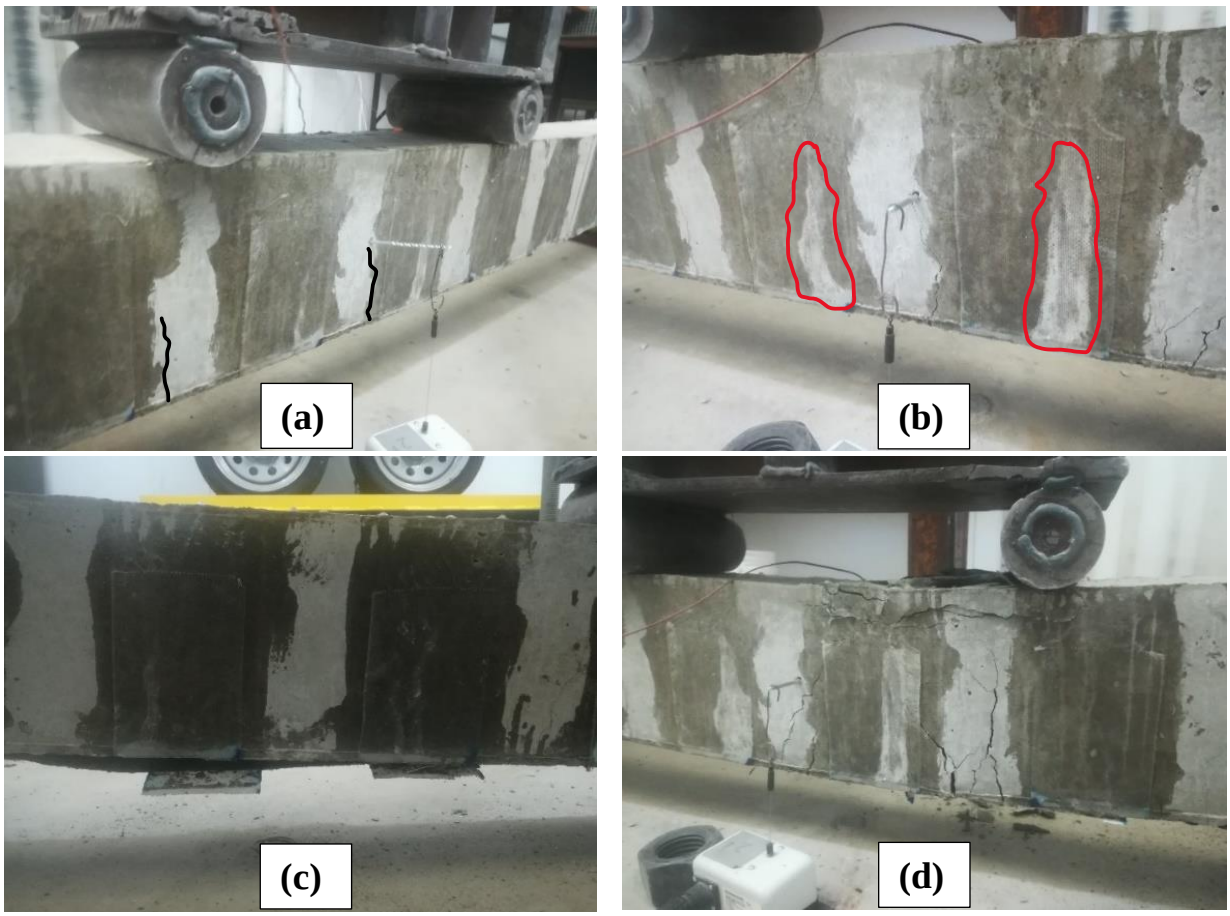

Figure 36. SBLTCT beam failure; (a) Flexural cracks, (b) Delamination of transverse FRP, (c) Debonding of longitudinal FRP and tearing of transverse FRP, (d) Concrete crushing.

Discussion of Results

The test results are summarized in Table 17 and the rest of this section discusses the key findings from the results of this study.

Table 17. Summary of results.

Load (kip) or displacement (in)	CBRT	CBCT	SBLRT	SBLCT	SBLTRT	SBLTCT
First cracking load	1.87	2.47	1.78	1.97	0.85	1.96
Displacement at first cracking load	0.11	0.12	0.12	0.06	0.03	0.05
Yielding of transverse FRP	-	-	-	-	9.42	12.56
Displacement at yielding of transverse FRP	-	-	-	-	1.18	1.66
Debonding of longitudinal FRP	-	-	10.09	10.89	9.36	12.17
Displacement at debonding of longitudinal FRP	-	-	1.11	1.20	1.66	2.37
Ultimate load	9.77	11.46	10.22	10.89	9.42	12.75
Displacement at Ultimate load	2.18	3.16	2.41	1.20	1.18	1.73

Effect of FRP Strengthening

The plots of the load vs. mid-span displacement for the control and strengthened beams are shown in Figure 37a-b, for both room and cold temperature testing conditions, respectively. It should be noted that the SBLTRT beam was accidentally preloaded prior to testing, and therefore was prematurely cracked prior to officially testing. To address this issue, an identical replacement beam was constructed and tested; however, there was technical issues with this beam test as well. The details of this additional beam are included in Appendix C. The original preloaded beam is included in the remaining discussion, as its behavior (beyond initial stiffness) followed the same patterns observed in the other beam tests.

The room temperature data in Figure 37 (a) shows that, the SBLRT beam exhibits a higher capacity than the CBRT beam at the point of 1.11 in. displacement where the longitudinal FRP

delaminates. From the SBLTRT, it can be seen that the complete delamination process is also delayed until 1.66 in. displacement (150% of SBLRT) because of the additional support from the transverse FRP. However, the ultimate capacity of the SBLTRT beam is lower than the other two beams, unlike the cold room data and contrary to what would be expected intuitively.

Figure 37 (b) shows that the SBLCT beam exhibits a higher capacity than the CBCT beam at the point of its FRP debonding (1.20 in. displacement), represented by a sudden dip in the data. Additionally, for the SBLTCT beam, the transverse FRP mitigates the process of the longitudinal FRP delamination and holds capacity until around 2.37 in. displacement (198% of only longitudinal FRP, SBLCT), and it has the highest capacity among these three beams. In summary, the behavior of the cold temperature beams is as predicted, and the results are promising for those considering FRP repairs on beams subjected to cold temperatures.

Another interesting result for both the room temperature and cold temperature FRP reinforced beams is that once the longitudinal wrap delaminates, the data then follows the data trends of the control beams rather closely. In fact, the lines follow each other almost exactly for the room temperature beams and at least at almost identical slopes for the cold temperature beams.

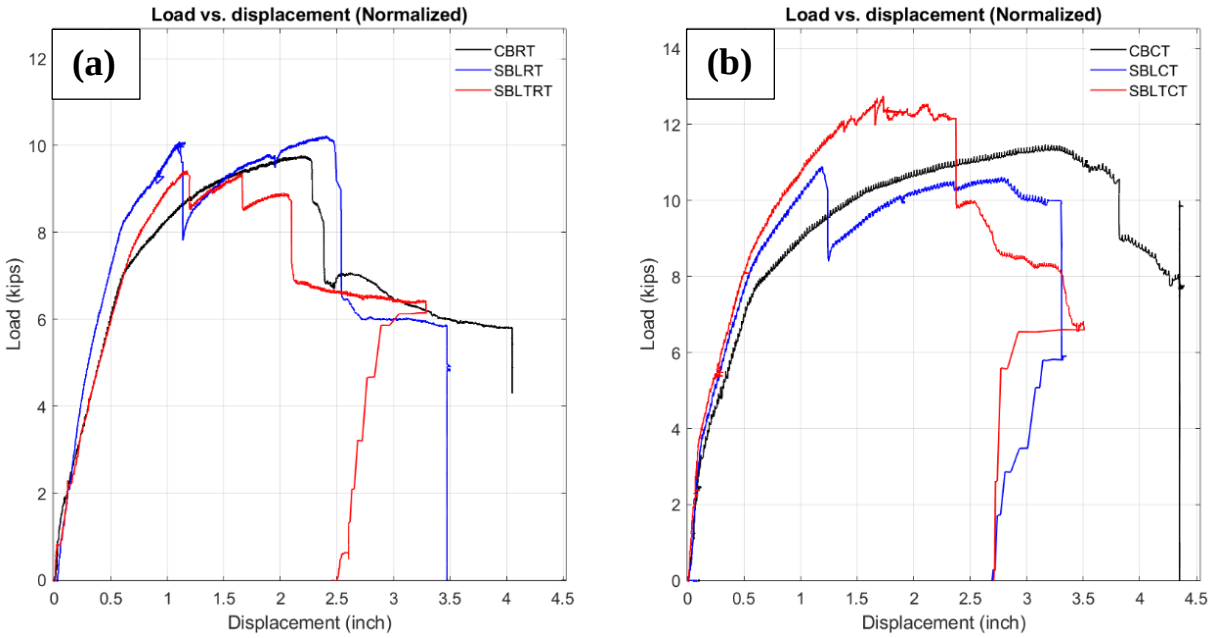

Figure 37. Load vs. displacement (at midspan) results for all beam types; (a) Room temperature, (b) Cold temperature.

The stiffnesses of the beams are compared in Figure 38 for both temperature conditions. As can be observed in Figure 38 (a), the SBLRT is the stiffest of the room temperature beams, over the majority of the curve. The SBLTRT and CBRT beams exhibited very similar stiffnesses as the loading increased. From the cold temperature data in Figure 38 (b), it can be seen that the SBLTCT beam exhibits larger stiffnesses along the entire graph compared to the SBLCT and CBCT beams, and the CBCT beam has the least stiffness among the three beams. These results indicate that the FRP reinforcement aided in increasing beam stiffnesses in both temperature conditions.

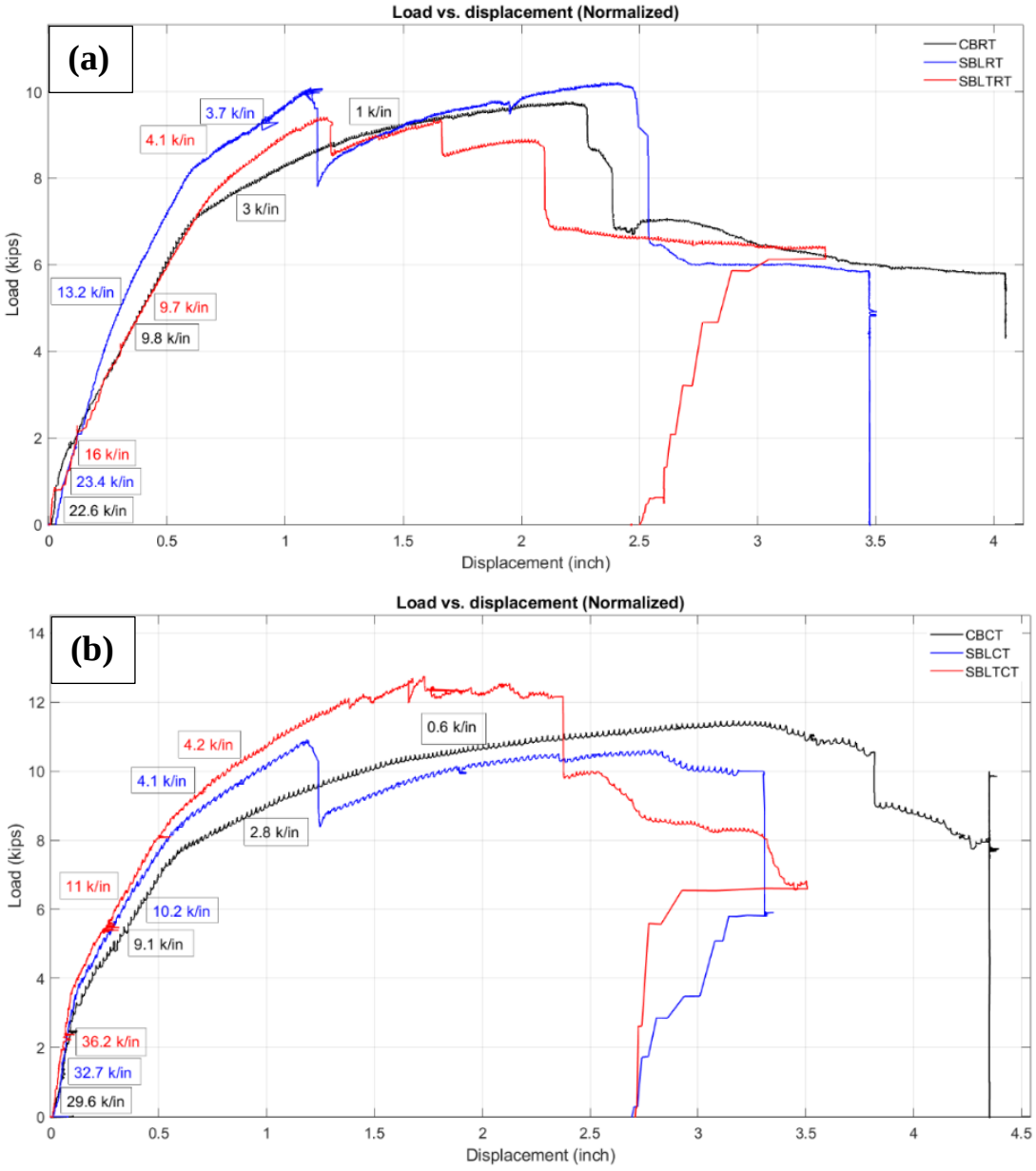

Figure 38. Stiffness results for all beam types; (a) Room temperature, (b) Cold temperature.

Effect of Temperature

To isolate the effects of temperature, the load vs. displacement relationships for each beam type are plotted in Figure 39a-c. As can be observed in Figure 39, the cold temperatures appear to have a positive effect on beam performance. The cold beams exhibited higher load carrying

capacities than the beams tested at room temperature for all three types. Additionally, FRP delamination occurred at larger displacements for the cold temperature beams than the room temperature beams. For example, FRP delamination of the SBLCT beam occurred at a displacement of 1.20 in., while FRP delamination of the SBLRT beam occurred at a displacement of 1.11 inch. In other words, SBLCT had an 8.11% higher displacement value than SBLRT at delamination. Similarly, SBLTCT beam delaminated at a displacement 42.77% higher than the SBLTRT beam, where the displacements were 2.37 in. and 1.66 in., respectively.

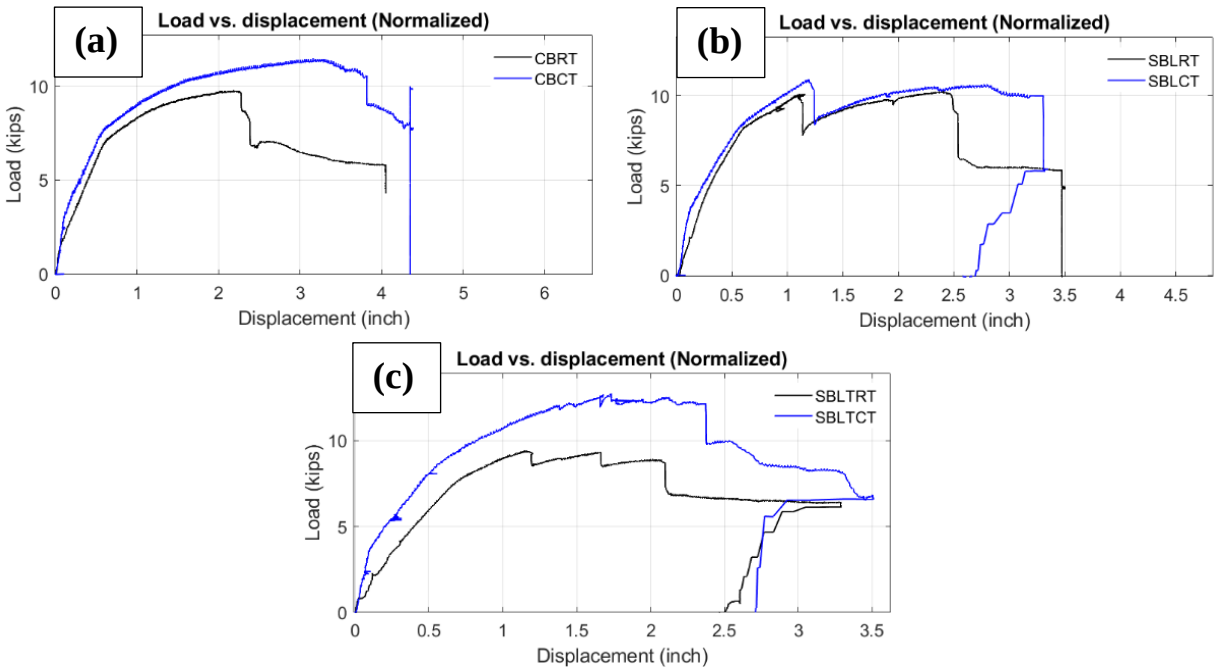

Figure 39. Load vs. displacement (at midspan) results for both temperature conditions; (a) Control beams, (b) Longitudinal strengthened beams, (c) Longitudinal + transverse strengthened beams.

The stiffness comparison between room temperature and cold temperature is shown in Figure 40. As previously discussed, the figure again shows that as loading increased, the stiffnesses decreased as expected. Comparing the stiffness values between the room and cold temperature beams, it can be seen that the initial stiffnesses are much higher for the cold temperature beams,

averaging a 35.4% increase from room temperature for the control and longitudinal strengthened beam types and a 126.25% increase for the longitudinal + transverse strengthened beam type (likely artificially over-increased by the unexpected SBLTRT results). Once the slopes/stiffnesses begin to change with higher load and higher displacements, the differences between room and cold temperature are less noticeable.

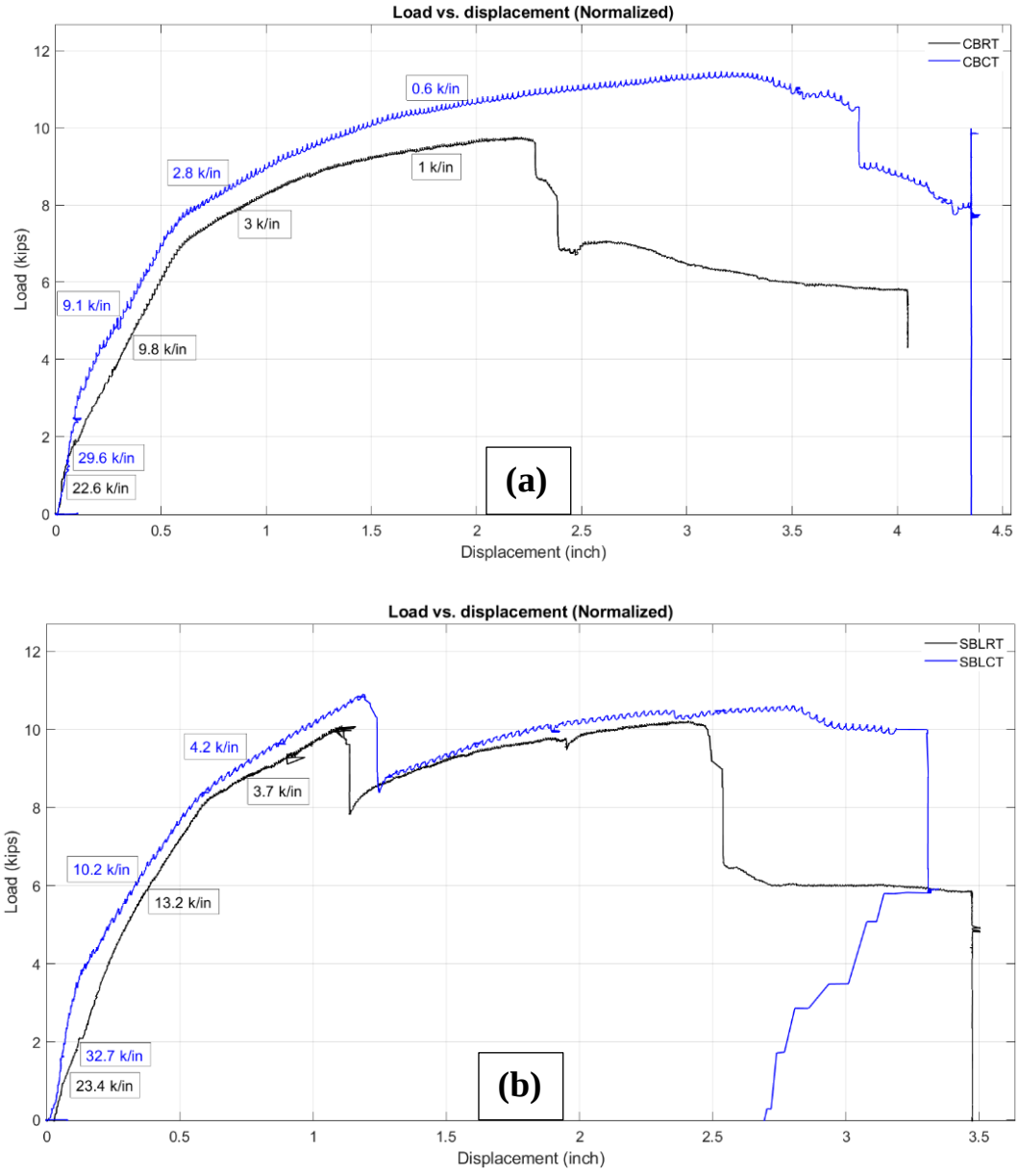

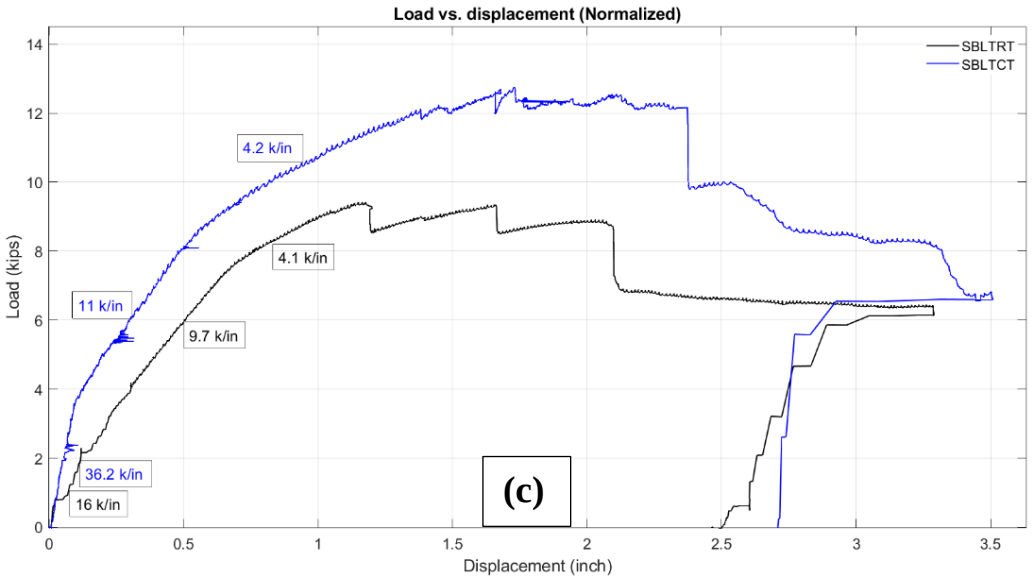

Figure 40. Stiffness results for both temperature conditions; (a) Control beams, (b) Longitudinal strengthened beams, (c) Longitudinal + transverse strengthened beams.

Predicted vs. Measured Results

A comparison between ACI predicted beam capacities and measured values are shown in Table 18. For the room temperature test conditions, the predicted beam capacity of the control beam was calculated as 7.34 kips, taking into account the actual f'_c of the concrete and following the ACI standards (details in Appendix A). From the experimental results, the ultimate capacity of CBRT was 9.77 kips, 33% higher than the ACI predicted capacity. The predicted capacity of the longitudinal strengthened beam was 11.58 kips and SBLRT had a lower ultimate capacity of 10.22 kips, 88% of the predicted capacity. The predicted capacity of the longitudinal + transverse strengthened beam was 11.53 kips and SBLTRT also had a lower ultimate capacity of 9.42 kips, 82% of the predicted capacity.

For the cold temperature test conditions, the predicted beam capacity of the control beam was 7.31 kips and CBCT had an ultimate capacity of 11.46 kips, 57% higher than the ACI predicted capacity. The predicted capacity of the longitudinal strengthened beam was 11.65 kips and SBLCT

had a lower ultimate capacity of 10.89 kips, 93% of the predicted capacity. The predicted capacity of the longitudinal + transverse strengthened beam was 11.59 kips and SBLTCT had an ultimate capacity of 12.75 kips, 10% higher than the predicted capacity. Overall, the ACI predicted capacities were quite conservative for the control beams and also under predicted the capacity of the longitudinal + transverse strengthened beam tested at cold temperature. However, the ACI calculations slightly overestimated the predicted capacities for the other strengthened beams at both room and cold temperatures. The last column of Table 18 represents what percent the measured capacity is of the predicted capacity, with values over 100% representing cases where the ACI calculations were conservative.

Table 18. Comparison of predicted and measured beam capacities.

Beam	**f'_c (psi)**	**Predicted beam capacity (kips)**	**Measured ultimate load (kips) (normalized)**	**Measured capacity % of predicted capacity**
CBRT	5990	7.34	9.77	133%
CBCT	4360	7.31	11.46	157%
SBLRT	5530	11.58	10.22	88%
SBLCT	6150	11.65	10.89	93%
SBLTRT	5140	11.53	9.42	82%
SBLTCT	5610	11.59	12.75	110%

The expected increases in beam capacities due to the FRP strengthening, as predicted by the ACI calculations, and compared with the measured changes in capacities, will be discussed here. The strengthened beams had a 54.91% higher predicted capacity than the control beam. However, the measured changes in capacities exhibited by the experimental results did not reach the 54.91% predicted increase. The predicted capacity of the strengthened beam was calculated using the modulus of elasticity of FRP from the coupon test. The coupons were made on a non-absorbent steel surface, and it is predicted that the epoxy resin had a better contribution to the FRP

coupon tensile strength, compared to the FRP applied to the RC beams. The surface of concrete is not impermeable (as was the steel for the coupon preparation) and the FRP application on the concrete beams required much more time than constructing the coupons. Since surface absorbency and pot life play important roles in FRP strength and FRP strengthened beam capacity, it is predicted that these were the reasons behind the test beams having a smaller measured increase in beam capacity than the hand calculation predicted increase for the strengthened beams compared to control. A summary of the predicted and measured changes in beam capacities due to FRP strengthening are shown in Table 19.

Table 19. Comparison of predicted and measured differences in beam capacities based on FRP strengthening.

Beam	**Predicted beam capacity (kips) (for f'_c = 4000 psi)**	**Predicted % difference (for f'_c = 4000)**	**Measured (normalized) beam capacity (kips)**	**Measured % difference**
CBRT	7.29	+ 54.91%	9.77	
CBCT			11.46	
SBLRT	11.30		10.22	+ 4.60%
SBLCT			10.89	- 3.58%
SBLTRT			9.42	- 4.97%
SBLTCT			12.75	+ 11.25%

Table 20 shows the predicted and measured changes in beam capacities due to cold temperature. The cold beams have a higher capacity than the room temperature beams for both predicted and measured results. However, the increases in capacities of measured beams is much higher than the predicted beam capacity increases. In other words, the increase in f'_c due to the concrete being frozen seems to have had a much larger effect on the physical test results (measured) than the hand calculations (predicted). In the calculation, only the change in the concrete compressive strength was considered. The cold temperature also affects the FRP tensile strength and the steel rebar yield strength, although these affects were not tested for in the current

study. The contribution of cold temperatures to the FRP and rebar strengths to the predicted beam capacity calculations may lead to similar capacity changes as the measured values.

Table 20. Comparison of predicted and measured increases in beam capacities based on cold temperature.

Beam	**f'_c (psi)**	**Predicted beam capacity (kips)**	**f'_c (psi) (cold)**	**Predicted beam capacity (kips) (for cold)**	**Predicted beam capacity increase**	**Measured ultimate load (kips) (normalized)**	**Measured beam capacity increase**
CBRT	5990	7.34	-	same	0.41%	9.77	17.30%
CBCT	4360	7.31	8161	7.37		11.46	
SBLRT	5530	11.58	-	same	2.94%	10.22	6.56%
SBLCT	6150	11.65	10730	11.92		10.89	
SBLTRT	5140	11.53	-	same	2.69%	9.42	35.35%
SBLTCT	5610	11.59	8860	11.84		12.75	

CHAPTER SIX

SUMMARY AND CONCLUSIONS

This chapter provides a brief summary of the research, followed by the conclusions that can be drawn. Some drawbacks of this study are also discussed, as well as recommendations for future research.

In this experimental study, material property testing was performed for the concrete and FRP strengthening materials and then the test series beams at two different temperatures were tested in four-point bending until failure. At each temperature, there was one control beam and two strengthened beams (longitudinal and longitudinal + transverse). Load vs. displacement graphs of the beams were plotted and the stiffnesses of the beams at both conditions were calculated and compared to each other. From the test results and calculated values, the following detailed conclusions are drawn.

- *With respect to tensile properties, CFRP significantly outperforms GFRP.*

From the tensile strength test results of FRP coupons, it can be said that CFRP has significantly higher yield strength and modulus of elasticity values than GFRP and these results are consistent with previous studies.

- *Low temperature has a positive effect on concrete compression strength.*

Comparing the concrete strength results of cylinders at both temperature conditions, it can be concluded that cold room cylinders showed an average of 87.18% increase in compressive strength compared to the cylinders at room temperature. This indicates a positive effect of low temperature on concrete compressive strength, which has been previously shown in other studies, but is confirmed here.

- *Overall, the FRP strengthening had positive effects on the RC beam behaviors in both room and cold temperatures.*

Comparing the ultimate load carrying capacity of control and strengthened beams at both temperatures, the longitudinal strengthened room and cold temperature beams had 17.87% and 13.56% higher load carrying capacities than the control beam counterparts at the point of longitudinal FRP debonding (at 1.11 in. and 1.20 in. displacement for room and cold temperature beams, respectively). Unlike the preloaded room temperature longitudinal + transverse strengthened beam, the cold temperature longitudinal + transverse strengthened beam had the highest load carrying capacity among the cold temperature beams at the point of FRP debonding, and it was 19.19% higher than the cold control beam.

- *Transverse wrapping significantly delayed the longitudinal FRP delamination at both room and cold temperature conditions.*

FRP delamination of longitudinal + transverse strengthened beams tested at room and cold temperatures occurred at 49.55% and 97.50% higher displacements, respectively, than the longitudinal only strengthened counterparts.

- *FRP strengthening increased the initial beam stiffnesses in both room and cold temperature conditions.*

From the comparison of initial stiffnesses of control and strengthened beams, the longitudinal strengthened room and cold temperature beams had 3.54% and 10.47% higher initial stiffnesses, respectively, than their control beam counterparts. Unlike the preloaded longitudinal + transverse strengthened beam at room temperature, the cold temperature longitudinal + transverse

strengthened beam had the highest initial stiffness among the cold temperature beams and was 22.30% stiffer than its control beam counterpart.

- *Testing at low temperature had a positive effect on the ultimate load carrying capacities of all beam types compared to testing at room temperature.*

All three cold beams showed higher load carrying capacities than their room temperature counterparts. The control cold beam had a 17.30% higher capacity than the room temperature control beam. Comparing the capacities of strengthened beams at both temperatures, longitudinal and longitudinal + transverse strengthened cold beams had 6.56% and 35.35% higher capacities than their room temperature counterparts, respectively.

- *Low temperature had a positive effect on the FRP delamination process.*

FRP delamination occurred later for the cold beams compared to their room temperature counterparts. The longitudinal and longitudinal + transverse strengthened cold beams were at 8.11% and 42.77% higher displacements at the point of delamination compared to the room temperature counterpart strengthened beams.

- *Low temperature had a positive effect on initial beam stiffnesses.*

Comparing the stiffness values (represented here by the slopes of the normalized load-displacement graphs), the cold beams had much higher stiffnesses than the room temperature beams during initial loading. More specifically, 30.97%, 39.74%, and 126.25% increases in stiffness were observed for control, longitudinal, and longitudinal + transverse strengthened beams, respectively. With increased load, the stiffnesses of the beams decreased. The differences in stiffness values between cold and room temperature beams also decreased with increased load.

- *The ACI calculated beam capacity predictions were quite conservative for the control beams, but slightly underestimated the strengthened beam capacities, excluding longitudinal + transverse tested in cold temperature conditions.*

The ultimate measured loads of the control beams at room and cold temperatures were 33% and 57% higher, respectively, than the ACI predicted capacity counterparts. The longitudinal strengthened beams exhibited ultimate loads at room and cold temperatures that were 88% and 93%, respectively, of the predicted capacity. Moreover, the ultimate measured load of the longitudinal + transverse beam at room temperature was 82% of its predicted capacity, but the longitudinal + transverse strengthened cold beam had a 10% higher ultimate load capacity than ACI predicted.

In summary, the low temperature had positive effects on the concrete compressive strengths, ultimate load carrying capacities of RC beams, FRP delamination, and the beam stiffnesses. The results are promising and further research on strengthening and repairing concrete structures with FRP is warranted for low temperature regions.

Drawbacks of the Current Study

Brief discussions on the drawbacks of this study are presented in the following bullets:

- The targeted low temperature was -40^{o}C for the cold beam testing. However, the minimum temperature of the trial beam never reached -40^{o}C, but rather had an average temperature of -38.77^{o}C through the depth. During testing, the average cold beam temperature was -31.50^{o}C. The temperature increase was caused by opening the door of the cold lab for both test setup and being able to observe the beam behaviors during testing. Although this is listed as a

drawback, realistically it simply means the temperature comparison performed in this study was between about -30°C (as opposed to -40°C) and room temperature.

- Shelf life/storing of epoxy resin is a key point of working with FRP and resin. It is very important to maintain the storage temperature and be mindful of the shelf life of epoxy resin after opening the container to avoid crystallization. If crystallization of epoxy resin occurs, proper measures according to the manufacturer should be adopted before using the material to ensure desired strength results and avoid introducing new variables into the research.
- The pot life of epoxy resin is another important property to keep in mind. Small batches of mixes should be made if the epoxy resin has a short pot life.
- Pre-loading was an issue for one beam in this study. Strain gauges and loading equipment should be properly checked before starting tests.

Recommendations for Future Research

Brief discussions on the recommendations for future research are discussed here. For future research on similar topics, it is suggested that more cylinders be made to accommodate performing more concrete strength tests on cold room cylinders to represent all batches of concrete and better quantify the increases in beam strengths.

The effect of cold temperature on FRP tensile strength and the steel rebar yield strength should be considered and included in the predicted beam capacity calculations to facilitate better comparisons with the measured experimental data. For example, if FRP tensile strength tests in cold temperatures were conducted, the results should be included in the predicted beam capacity calculations for a more accurate representation of the strengthened beam capacity in cold temperature conditions. One study that has discussed the effects of cold temperature on FRP tensile

strength is briefly discussed here for additional insight. Dutta and Hui (1996) studied the internal stresses in composites of polymeric materials at low temperature. They tested a glass composite material and found increased Young's modulus and shear modulus with the reduction of temperature and similar positive effects may occur for the materials used in the present study. Cold temperature testing of additional FRP coupons is a recommendation for future research and the MTS Criterion C43, a benchtop mechanical testing system with an environmental chamber, housed in the Subzero Structures Laboratory at MSU could be used.

Finally, freeze-thaw cycling tests and/or low load fatigue tests of both control and strengthened beams at both cold and room temperature conditions would be an important extension of the present study and are also recommended for future research. Exploring these two topics in particular would further shed light on the overall behavior of FRP strengthened RC beams and better facilitate the potential for FRP repairs to be used more abundantly in cold temperature applications, for example, bridge beams in Montana.

REFERENCES CITED

Abbas, Z., & Shahadat, F. (2015). Use of FRP composite for strengthening of concrete structures. 636–640.

ACI 318. *Building Code Requirements for Structural Concrete (ACI 318-19) and Commentary (ACI 318R-19),* American Concrete Institute, 2019.

ACI 440.2R-17: *Guide for the Design and Construction of Externally Bonded FRP Systems for Strengthening Concrete Structures*. (2017). American Concrete Institute. https://doi.org/10.14359/51700867

Aiswarya, A., & Prabhakaran, P. (2017). A Review on Strengthening of RC Beams Using Near Surface Mounted (NSM). *International Journal of Innovative Research in Science, Engineering and Technology*, *6*(4), 60–64.

Alaskan Way Viaduct: https://en.wikipedia.org/wiki/Alaskan_Way_Viaduct

Alkhrdaji, T., Nanni, A., Chen, G., and Barker, M. (1999). "Solid RC Decks Strengthened with FRP," *Concrete International*, 21(10), 37-41.

ASTM International. C143/C143M-20 Standard Test Method for Slump of Hydraulic-Cement Concrete. West Conshohocken, PA; *ASTM International*, 2020. doi: https://doi.org/10.1520/C0143_C0143M-20

ASTM International. C150/C150M-20 Standard Specification for Portland Cement. West Conshohocken, PA; *ASTM International*, 2020. doi: https://doi.org/10.1520/C0150_C0150M-20

ASTM International. C31/C31M-21 Standard Practice for Making and Curing Concrete Test Specimens in the Field. West Conshohocken, PA; *ASTM International*, 2021. doi: https://doi.org/10.1520/C0031_C0031M-21

ASTM International. C39/C39M-21 Standard Test Method for Compressive Strength of Cylindrical Concrete Specimens. West Conshohocken, PA; *ASTM International*, 2021. doi: https://doi.org/10.1520/C0039_C0039M-21

ASTM International. C78-02 *Standard Test Method for Flexural Strength of Concrete (Using Simple Beam with Third-Point Loading).* West Conshohocken, PA, 2002. doi: https://doi.org/10.1520/C0078-02

ASTM International. D3039/D3039M-17 Standard Test Method for Tensile Properties of Polymer Matrix Composite Materials. West Conshohocken, PA; *ASTM International*, 2017. doi: https://doi.org/10.1520/D3039_D3039M-17

Attari, N., Amziane, S., & Chemrouk, M. (2012). Flexural strengthening of concrete beams using CFRP, GFRP and hybrid FRP sheets. *Construction and Building Materials*, *37*, 746–757. https://doi.org/10.1016/j.conbuildmat.2012.07.052

Balendran, R. V., Rana, T. M., Maqsood, T., & Tang, W. C. (2002). Application of FRP bars as reinforcement in civil engineering structures. *Structural Survey*, *20*(2), 62–72. https://doi.org/10.1108/02630800210433837

Bank, L. C. (2006). Application of FRP Composites to Bridges in the USA. *Proceedings of the International Colloquium on Application of FRP to Bridges*, *1*, 9–16. http://www.researchgate.net/profile/Lawrence_Bank/publication/234094998_Application_of_FRP_Composites_to_Bridges_in_the_USA/links/0912f50f3507d4cb89000000.pdf

Baumert, M.E., Green, M.F., and Erki, M.A. (1996). Low temperature behaviour of concrete beams strengthened with FRP sheets. *Proceedings of the 1996 CSCE Annual Conference*, Edmonton, Alta., pp. 179–190.

Bradberry, TE and Wallace, S (2003). FRP Reinforced Concrete in Texas TransportationPast, Present, Future. Field Applications of FRP Reinforcement: Case Studies. Editors: Sami Rizkalla and Antonio Nanni. *ACI International* SP-215, 2003, pp.3-35.

Carmichael, B. M., & Barnes, R. W. (2005). Repair Of The Uphapee Creek Bridge With FRP (Issue November 2005).

Chawla, K. K. (2011). Composite materials science and engineering. In *Composites* (Vol. 20, Issue 3). https://doi.org/10.1016/0010-4361(89)90346-7

Ching Chiaw Choo, Tong Zhao, & Issam E. Harik. (2007). Retrofit Of The Louisa-Fort Gay Bridge Using CFRP Laminates.

Chołostiakow, S., & Kotynia, R. (2014). Flexural strengthening of RC beams by using a near surface mounted T-section profiles. *Budownictwo i Architektura*, *13*(3), 071–078. https://doi.org/10.35784/bud-arch.1767

Church road bridge: https://compositesuk.co.uk/construction-sector-group

Crystalized epoxy resin: https://images.app.goo.gl/n5gQttq8ttQhThcL9

Dutta, P.K., and Hui, D. (1996). Low-Temperature and Freeze-Thaw Durability of Thick Composites. Composites Part B: Engineering, 27(3-4): 371-379.

Ehsani, B. M., Farahani, M., & Raatz, E. (2012). repair of columns with FRP laminates. *Structure Magazine*, *January*, 35–37.

El-Hacha, R., Wight, R. G., & Green, M. F. (2004). Prestressed Carbon Fiber Reinforced Polymer Sheets for Strengthening Concrete Beams at Room and Low Temperatures. *Journal of Composites for Construction*, *8*(1), 3–13. https://doi.org/10.1061/(asce)1090-0268(2004)8:1(3)

FibreGlast: http://www.uscomposites.com/

Ghaffary, A., & Moustafa, M. A. (2020). Synthesis of repair materials and methods for reinforced concrete and prestressed bridge girders. *Materials*, *13*(18). https://doi.org/10.3390/ma13184079

Gomez J, Casto B (1996). Freeze-Thaw Durability of Composite Materials. In: Ehsani MR (ed) Fiber Composites in Infrastructure: *Proceedings of the First International Conference in Infrastructures*, Tucson, AZ, 15-17 January 1996.

Green, M. F., Bisby, L. A., Beaudoin, Y., & Labossière, P. (2000). Effect of freeze-thaw cycles on the bond durability between fibre reinforced polymer plate reinforcement and concrete. *Canadian Journal of Civil Engineering*, *27*(5), 949–959. https://doi.org/10.1139/cjce-27-5-949

Hadi, M.N.S. (2003). Retrofitting of Shear Failed Reinforced Concrete Beams. *Composite Structures*, 62: 1-6

Harichandran, R & Baiyasi, M. (2000). Repair of Corrosion-Damaged Columns Using FRP Wraps. Research Report RC-1386, Michigan Department of Transportation, Lansing, MI.

Hawileh, R. A., Rasheed, H. A., Abdalla, J. A., & Al-Tamimi, A. K. (2014). Behavior of reinforced concrete beams strengthened with externally bonded hybrid fiber reinforced polymer systems. *Materials and Design*, *53*, 972–982. https://doi.org/10.1016/j.matdes.2013.07.087

Hosen, M. A., Jumaat, M. Z., Alengaram, U. J., Islam, A. B. M. S., & Hashim, H. bin. (2016). Near surface mounted composites for flexural strengthening of reinforced concrete beams. *Polymers*, *8*(3). https://doi.org/10.3390/polym8030067

Hosny, A., Shaheen, H., Abdelrahman, A., & Elafandy, T. (2006). Performance of reinforced concrete beams strengthened by hybrid FRP laminates. *Cement and Concrete Composites*, *28*(10), 906–913. https://doi.org/10.1016/j.cemconcomp.2006.07.016.

Julio F. Davalos, Karl E. Barth, Indrajit Ray, Chunfu Lin, & Brayack, D. A. (2006). District 3-0 Investigation Of Fiber-Wrap Technology For Bridge Repair And Rehabilitation (Phase-I).

Kelly, C. (2018). Higgins Avenue Bridge Rehabilitation.

Khalifa, A. M. (2016). Flexural performance of RC beams strengthened with near surface mounted CFRP strips. *Alexandria Engineering Journal*, *55*(2), 1497–1505. https://doi.org/10.1016/j.aej.2016.01.033

McCormick, F.C., 1972, "Why not Plastic Bridges," *J. of Structural Division*, ASCE, Vol. 98, pp. 1757-1767.

Morsy, A., & Mahmoud, E. T. (2013). Bonding techniques for flexural strengthening of R.C. beams using CFRP laminates. *Ain Shams Engineering Journal*, *4*(3), 369–374. https://doi.org/10.1016/j.asej.2012.11.004

Nezamian, A., & Setunge, S. (2004). A case study of application of FRP composites in strengthening of the reinforced concrete headstock of a bridge structure. *FRP Composites in Civil Engineering - CICE 2004*, *11*(5), 939–945. https://doi.org/10.1201/9780203970850.ch107

Parretti, R. Nanni, A. Cox, J. Jones, C. and Mayo, R. (2003). Flexural Strengthening of Impacted PC Girder with FRP Composites. Field Applications of FRP Reinforcement: Case Studies. Editors: Sami Rizkalla and Antonio Nanni, 2003. *ACI International SP215*, pp.249-261.

Pham, T. M., & Hao, H. (2016). RC beams strengthened with longitudinal and U-wrap FRP. *Proceedings of the 8th International Conference on Fibre-Reinforced Polymer (FRP) Composites in Civil Engineering, CICE 2016*, 1356–1361.

Prota, A., Nanni, A., Manfredi, G., & Cosenza, E. (2000). Seismic Upgrade of Beam-Column Joints with FRP Reinforcement. 1–17, *Industria Italiana del Cemento*, Nov. 2000

Purfleet Footbridge: https://lifespanstructures.com/purfleet-footbridge/

Sadone, R., Quiertant, M., Ferrier, E., Chataigner, S., & Mercier, J. (2013). *Anchoring FRP laminates for the seismic strengthening of RC columns*.

Sahawany M., Arockiasamy M., Beitelman T. and Sowrirajan R. (1996). Reinforced Concrete Rectangular Beams Strengthened with CFRP Laminates. *Composites*, 27(B): 225-233

Sarafraz, M., & Danesh, F. (2011). Use near surface mounted FRP rods for flexural retrofitting of RC columns. *Advances in FRP Composites in Civil Engineering - Proceedings of the 5th International Conference on FRP Composites in Civil Engineering, CICE 2010*, 833–836. https://doi.org/10.1007/978-3-642-17487-2_183

Sen, R. (2003). Advances in the application of FRP for repairing corrosion damage. *Progress in Structural Engineering and Materials*, *5*(2), 99–113. https://doi.org/10.1002/pse.147

Shahrooz, B. M., Boy, S. (2004). “Retrofit of a Three-Span Slab Bridge with Fiber Reinforced Polymer Systems—Testing and Rating,” *Journal of Composites for Construction, ASCE*, 8(3), 241-247.

Shrivastava, R., Gupta, U., & Choubey, U. B. (2009). FRP: Research, Education and Application in India and China in Civil Engineering. *International Journal of Recent Trends in Engineering*, *1*(6), 89–93.

Soudki KA & Green MF. (1996). Performance of CFRP Retrofitted Concrete Columns at Low Temperatures. In: El-Badry MM (ed). *Advanced Composite Materials in Bridges and Structures: 2nd International Conference*, Montreal Quebec, 11-14 August 1996. Montreal: Canadian Society for Civil Engineering. 1996: 427-434

Soudki, K. A. & Green MF (1997). “Freeze-thaw response of CFRP wrapped concrete.” *Concrete International*, 19(8), 64-67.

Tang, B. (1997). Fiber Reinforced Polymer Composites Applications in USA Dot - Federal Highway Administration. *Guide to Stability Design Criteria for Metal Structures (6th Edition)*, 128–204. https://doi.org/10.1525/hlq.2007.70.2.plates

Toutanji H. and El-Korchi T. (1998). Durability Characteristics of Concrete Beams Externally Bonded with FRP Composites Sheets. *2nd International Conference on Composites in Infrastructure*, Tuscon, AZ, 1998.

Omega Engineering Inc. (Thermocouple): https://images.app.goo.gl/rH83Vhu9VcvKcz3F6

US Composite: http://www.uscomposites.com/

Wenwei, W., & Guo, L. (2006). Experimental Study of RC Beams Strengthened with CFRP Sheets Under Sustaining Loads. *Journal of Wuhan University of Technolog*, *21*(3), 28–31.

APPENDICES

APPENDIX A

HAND CALCULATIONS FOR BEAM CAPACITIES

Appendix A is devoted to the theoretical background of designing and analyzing the flexural behavior of the RC beams following ACI 318-19. It also describes the step by step process of calculating the nominal moment strength (M_n) of both control and FRP strengthened beams.

Hand Calculations for Control Beam Capacity

The flexure theory of RC beams is mainly based on some basic assumptions made for simplification (JKW textbook). The assumptions are as follows:

a) Plane sections remain plane.

b) The strain in the reinforced bar and concrete are equal at the same level. This assumption ensures that the concrete and reinforcement act together to carry load.

c) The tensile strength of the concrete is neglected.

d) The maximum concrete strain at extreme concrete compression fiber (ε_c) is equal to 0.003.

e) The stresses in the concrete and reinforcement can be measured from the strains.

The loading of the beam is shown in Figure 41, as well as the shear and bending moment diagrams. The positive moment generated from the loading causes compression on the top surface of the beam and tension on the bottom surface.

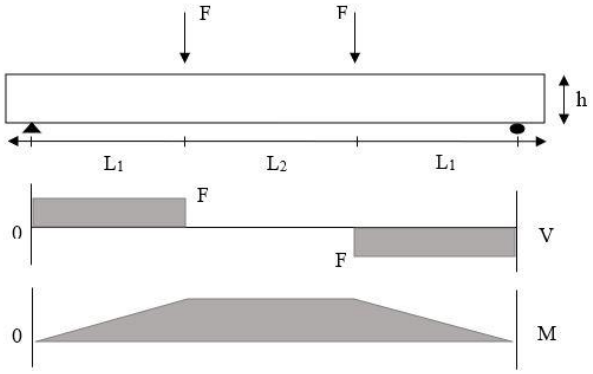

Figure 41. Schematic diagram of loading on beam (top), shear force V (middle), and bending moment M (bottom) diagrams.

According to section 22.2.2.4 ACI 318-19, a further simplification permits an equivalent rectangular concrete stress distribution (commonly referred to as the Whitney stress block, see Figure 42) to be used for calculating the nominal flexural strength. A stress of $0.85f'_c$ is distributed on the concrete uniformly over the depth of the Whitney stress block, "a", equal to $\beta_1 c$, where c is the neutral axis distance from the top and β_1 is a reduction factor and is a function of f'_c.

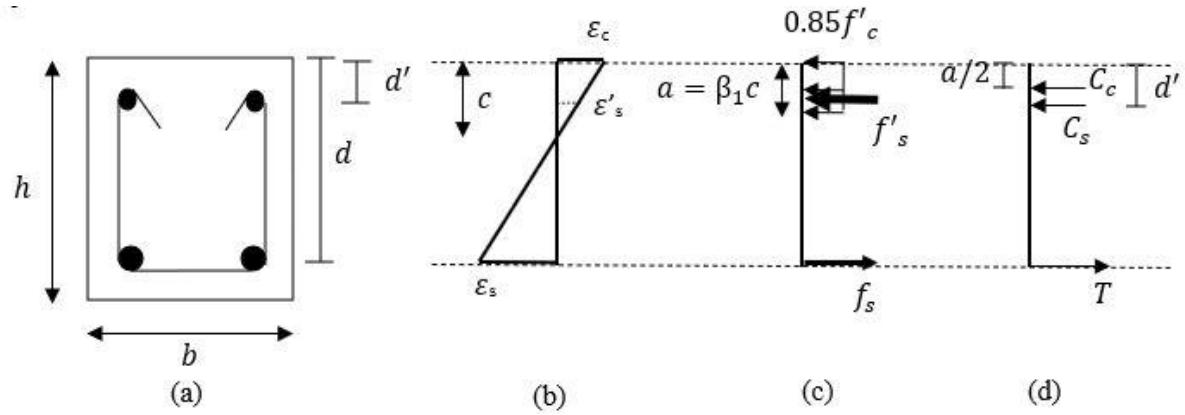

Figure 42. (a) Cross section of control beam, (b) Strain distribution, (c) Stress distribution, (d) Internal force distribution.

The reinforcement areas of the compression and tension zones are A'_s and A_s, respectively. Additionally, ε_s and f_s are the strain and stress, respectively, in the tension reinforcement and the strain and stress in the compression reinforcement are ε'_s and f'_s, respectively. The flexural strength calculation is made assuming f_s is equal to f_y, the yield stress of the reinforcement. The compression forces in the concrete and reinforcement can be expressed as C_c and C_s, respectively, and are calculated with Eqn. 1 and 2, and the tension force in the tension reinforcement is T, calculated with Eqn. 3.

$$C_c = 0.85f'_c ab \quad \text{(Eqn. 1)}$$

$$C_s = A'_s(f'_s - 0.85f'_c) \quad \text{(Eqn. 2)}$$

$$T = A_s f_s \quad \text{(Eqn. 3)}$$

The equilibrium equation can be represented by Eqn. 4 and depth of stress block, a and depth of neutral axis, c are calculated with Eqn. 5 and 6 respectively.

$$T = C_c + C_s \quad \text{(Eqn. 4)}$$

$$a = \frac{A_s f_s + A'_s(0.85 f'_c - f'_s)}{0.85 f'_c b} \quad \text{(Eqn. 5)}$$

$$c = \frac{a}{\beta_1} \quad \text{(Eqn. 6)}$$

Where, the factor for compression stress block, β_1, can be calculated as follows (from Table 22.2.2.4.3, ACI 318-19):

a) $\beta_1 = 0.85$ for 2500 psi $\leq f'_c \leq$ 4000 psi

b) $\beta_1 = 0.85 - \frac{0.05(f'_c - 4000)}{1000}$ for 4000 psi $< f'_c <$ 8000 psi

c) $\beta_1 = 0.65$ for $f'_c \geq$ 8000 psi

The nominal flexural strength can be calculated by multiplying the internal forces with their moment arm, summing the moments about a location in the cross-section, and setting equal to zero for equilibrium (Eqn. 7). Taking the moment about the point of the compression force in concrete, it can be written as,

$$M_n = T\left(d - \frac{a}{2}\right) - C_s(d' - \frac{a}{2}) \quad \text{(Eqn. 7)}$$

For the loading here (previously shown in Figure 41), the load, P, required to induce M_n, is calculated with Eqn. 8:

$$P = \frac{M_n \times 6}{L} \quad \text{(Eqn. 8)}$$

The strain in the tension reinforcement, ε_s, can be calculated using similar triangles of the strain distribution diagram (Eqn. 9). With this calculated value, the assumption that the tension

steel yields can be checked if the strain in the tension reinforcement is greater than the yield strain (ε_y). ε_y is calculated with Eqn. 10, where, E_y is the modulus of elasticity of steel:

$$\varepsilon_s = \frac{d-c}{c} \times \varepsilon_c \quad \text{(Eqn. 9)}$$

$$\varepsilon_y = \frac{f_y}{E_y} \quad \text{(Eqn. 10)}$$

The flexural tension cracking occurs when the stress in the extreme tension fiber reaches the modulus of rupture (f_r). The moment that causes this stress is called the cracking moment (M_{cr}), which is calculated with Eqn. 11, where, I_g and y_t are the moment of inertia and the centroid of the section, respectively. The modulus of rupture, f_r is equal to $7.5\sqrt{f'_c}$.

$$M_{cr} = \frac{f_r \times I_g}{y_t} \quad \text{(Eqn. 11)}$$

There is a sudden change in tension force from concrete to the rebar in the tension zone which can cause a brittle failure. To prevent this failure mode, the requirement of minimum reinforcement, described in section 9.6.1.2, ACI 318-19, should be met. Also, the minimum flexural strength of the beam should be equal to or greater than the cracking moment strength.

Hand Calculations for Strengthened Beam Capacity

The flexural strength of RC beams strengthened externally with FRP wrapping on the tension face can be calculated by following the standard ACI 440.2R-17. The following assumptions are made in calculating the strength:

a) The maximum compressive strain of concrete (ε_c) is 0.003 and the tensile strength of the concrete is neglected.
b) There is no relative slip between the FRP layer and the concrete.

c) The FRP reinforcement has a linear elastic stress-strain relationship to failure.

d) Plane sections remain plane before and after loading. The strain in the rebar and concrete are directly proportional to their distance from the neutral axis (a function of c).

Figure 43 shows the cross section of an FRP strengthened beam as well as the strain, stress, and force distributions. For a further simplification of the calculations, the terms α_1 and β_1 are introduced that define the rectangular stress block in the concrete which is equivalent to the nonlinear distribution of stress. α_1 and β_1 can be calculated following the ACI 318-19 standard if the concrete crushing failure mode controls. To represent the parabolic stress-strain relationship of concrete, α_1 and β_1 equations can be written as:

$$\alpha_1 = \frac{3\varepsilon_c'\varepsilon_c - {\varepsilon_c}^2}{3\beta_1{\varepsilon_c'}^2} \quad \text{(Eqn. 12)}$$

$$\beta_1 = \frac{4\varepsilon_c' - \varepsilon_c}{6\varepsilon_c' - 2\varepsilon_c} \quad \text{(Eqn. 13)}$$

Where, ε_c' is the strain corresponding to the compressive strength of concrete, f_c', and can be expressed as $\frac{1.7f'_c}{E_c}$ and ε_c is the concrete strain at failure.

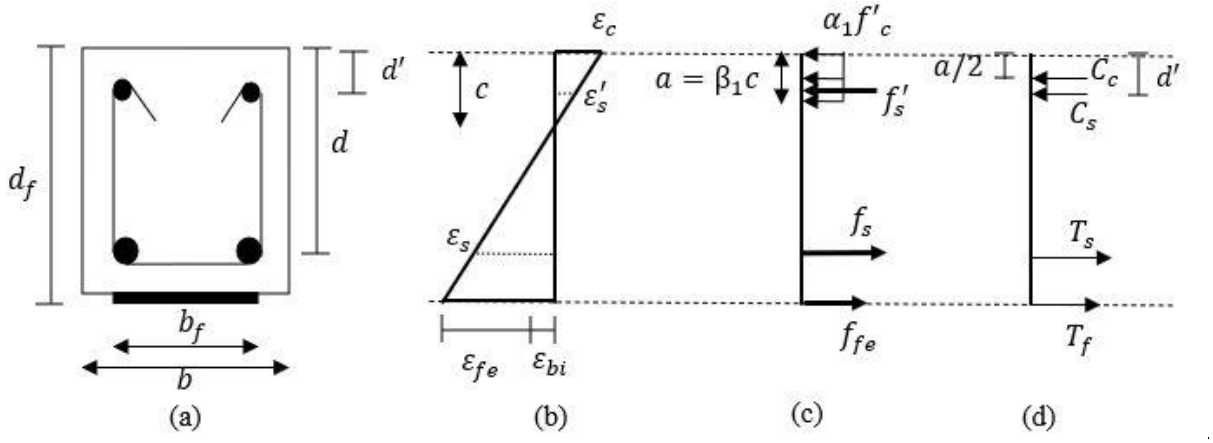

Figure 43. (a) Cross section of strengthened beam, (b) Strain distribution, (c) Stress distribution, (d) Internal force distribution.

This strength calculation is an iterative process that starts with an assumption of the location of the neutral axis, c. According to ACI, the reasonable initial assumed c could be $0.2d$. The width and thickness of the FRP layer are b_f and t_f, respectively. The environmental effect, C_E (according to T 9.4, ACI 440.2R-17) should include the FRP strain (ε_{fu}) and stress (f_{su}). The debonding and effective strains can be expressed as ε_{fd} and ε_{fe} and are shown in Eqn. 14 and 15 respectively with E_f as the modulus of elasticity of the FRP.

$$\varepsilon_{fd} = 0.083\sqrt{\frac{f_c'}{n\mathrm{E}_f\mathrm{t}_f}} \leq 0.9\varepsilon_{fu} \quad \text{(Eqn. 14)}$$

$$\varepsilon_{fe} = 0.003 \times \frac{\mathrm{d}_f - c}{c} - \varepsilon_{bi} \leq \varepsilon_{fd} \quad \text{(Eqn. 15)}$$

Where, n is the number of FRP layers and ε_{bi} is the initial strain at the time the FRP is applied, negligible in the case of this research. Similar triangles are used and ε_c, ε_s, and ε'_s are shown in Eqn. 16, 17, and 18 respectively. The Stress in FRP, f_{fe} is calculated with Eqn. 19.

$$\text{Strain in concrete, } \varepsilon_c = \varepsilon_{fe} \times \frac{c}{\mathrm{d}_f - c} \quad \text{(Eqn. 16)}$$

$$\text{Strain in tension rebar, } \varepsilon_s = \varepsilon_{fe} \times \frac{d - c}{\mathrm{d}_f - c} \quad \text{(Eqn. 17)}$$

$$\text{Strain in compression rebar, } \varepsilon'_s = \varepsilon_{fe} \times \frac{c - d\prime}{\mathrm{d}_f - c} \quad \text{(Eqn. 18)}$$

And:

$$\text{Stress in FRP, } f_{fe} = E_f\varepsilon_{fe} \quad \text{(Eqn. 19)}$$

From the equilibrium of the section, the summation of forces can be written as:

$$C_s + C_c = T_s + T_f \quad \text{(Eqn. 20)}$$

Depth of stress block, a and depth of neutral axis, c are calculated with Eqn. 21 and 22 respectively.

$$a = \frac{A_s f_s + A_f f_{fe} - A'_s f'_s + \alpha_1 f'_c A'_s}{\alpha_1 f'_c b} \quad \text{(Eqn. 21)}$$

$$c = \frac{a}{\beta_1} \quad \text{(Eqn. 22)}$$

Where, A_s and A'_s are the reinforcement areas of the tension and compression zones and A_f is the area of the FRP. The calculated c from eqn. 22 is then compared with the assumed c. If they do not agree, the assumed c needs to be modified and the steps are repeated until they match. The nominal flexural strength (M_n) is calculated, considering the contribution of steel reinforcement (M_{ns}) and the contribution of the FRP (M_{nf}) which are calculated with Eqn. 23 and 24 respectively. M_n is calculated with Eqn. 25. An additional reduction factor ($\Psi_f = 0.85$) is applied to the FRP.

$$M_{ns} = A_s f_s \left(d - \frac{a}{2}\right) - A'_s f'_s (d' - \frac{a}{2}) \quad \text{(Eqn. 23)}$$

$$M_{nf} = A_f f_{fe} \left(d_f - \frac{a}{2}\right) \quad \text{(Eqn. 24)}$$

$$M_n = M_{ns} + \Psi_f M_{nf} \quad \text{(Eqn. 25)}$$

In summary, the flexural capacity of an FRP strengthened beam is calculated following the flowchart shown in Figure 44.

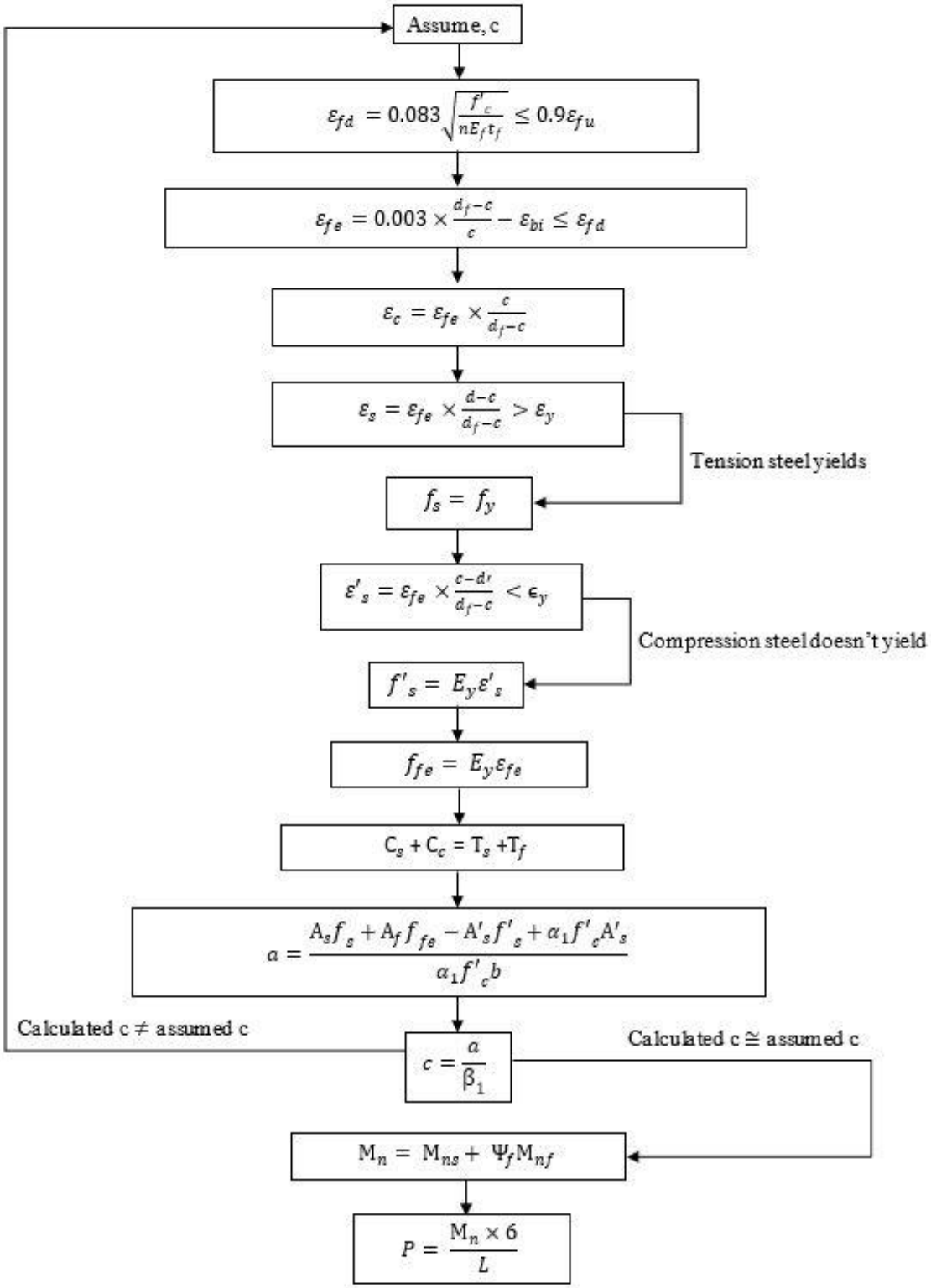

Figure 44. Flowchart of calculating flexural capacity of FRP strengthened beam.

APPENDIX B

THERMAL BEHAVIOR OF CONCRETE BEAM

Appendix B is devoted to a discussion on a trial beam constructed for this research and used to determine the appropriate testing protocol for the cold temperature beams. A 3 ft long rectangular (6 in. × 8 in.) beam was made initially to see how the temperature of the concrete specimen decreases after being in the cold room and how it warms up with time after being taken out of the cold lab. Since temperature change is a function of time, this test was necessary to determine how quickly the concrete warms up and whether the test series beams would have time to be tested before reaching temperatures outside of the intended cold temperature window. The overall goal is to keep track of how quickly the beam warms up to determine whether it is suitable to test the cold beams with the room temperature test setup, where the load frame, actuator, etc. are housed and already setup for use, or if the beams needed to be tested in the cold lab to ensure appropriate beam temperatures throughout testing.

The same mix design was used for making the trial beam as the main beams, following Table 6. Three T-type thermocouple wires were placed at the top (T), middle (M), and bottom (B) of the beam to have continuous results. The top and bottom thermocouples were put at 1 inch from the top and bottom edges (see Figure 45). Figure 46 shows the cross section and the top view of the beam.

Figure 45. Formwork setup of the trial beam, showing thermocouple locations.

Figure 46. Trial beam; cross section (left) and top view (right).

Firstly, the cold lab room temperature was set to -40^{o}C. It took the room temperature around 31 hours to get close to -40^{o}C (-38.24^{o}C) for the first time. It hit -40^{o}C after 73 hours. The lowest temperature of the room was -40.31^{o}C. The trial beam was taken into the cold room after 33 hours of cooling, when the room temperature was -38.20^{o}C and the beam temperatures measured 17.88^{o} C (T), 17.28^{o}C (M) and 16.82^{o}C (B) before the beam was placed in the room. It took the beam around 18 hours to get close to the minimum for the first time and the temperatures were -38.02^{o}C (T), -38.08^{o}C (M) and -38.12^{o}C (B). The beam temperatures hit the minimum after 38 hours at -38.67^{o}C (T), -38.76^{o}C (M) and -38.88^{o}C (B). Figure 47 shows the time vs. temperature data, with the room temperature data shown in the top plot and the beam temperature data shown in the bottom plot.

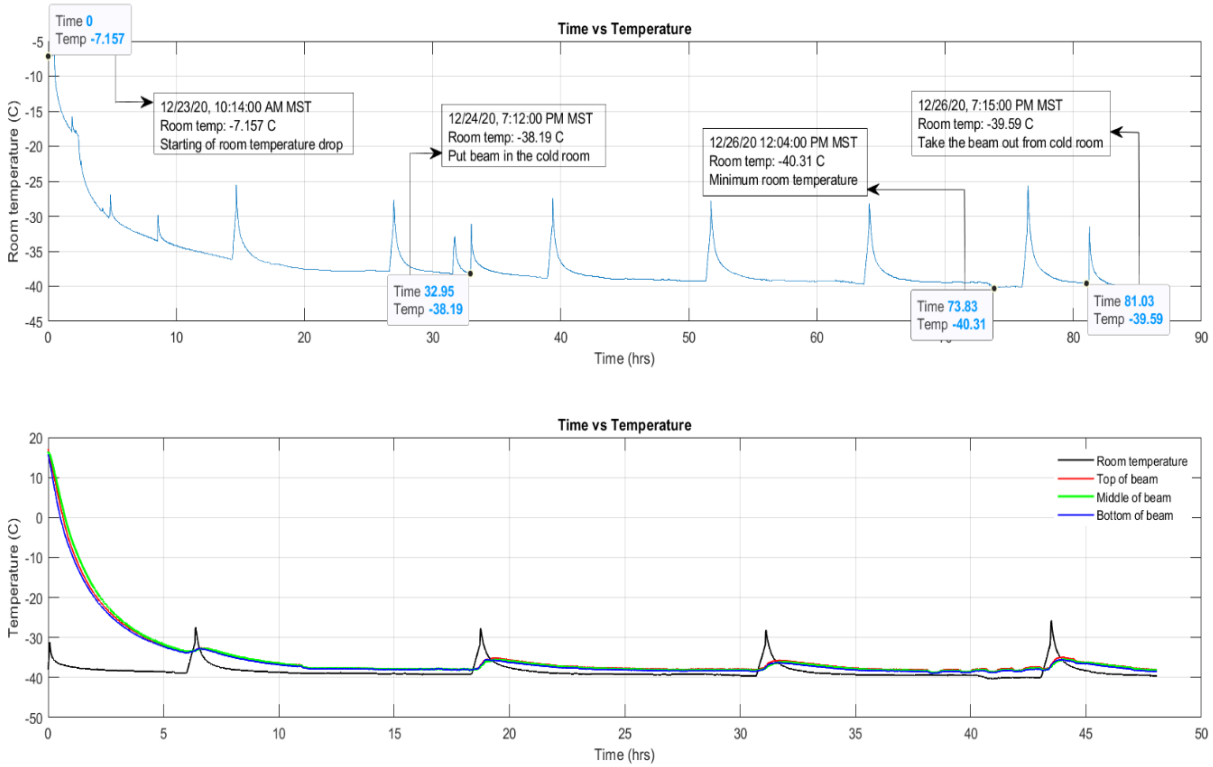

Figure 47. Temperature vs. Time data; room temperature starting at the initial cold room temperature set time (top) and beam temperature starting at the time beam was placed in cold room (bottom).

The beam temperatures were -38.06°C (T), -38.27°C (M) and -38.51°C (B) just before taking it out of the cold room. Some key data after the beam was moved to room temperature are shown in Table 21 and the time vs. beam temperature is shown in Figure 48. The temperature curve starts plateauing after 20 hours.

Table 21. Beam temperatures vs. time after removing from cold room.

Time (min)	Top	Middle	Bottom
15	-32.05°C	-34.01°C	-31.54°C
30	-25.92°C	-28.60°C	-25.83°C
45	-20.91°C	-23.77°C	-21.24°C
60	-16.68°C	-19.59°C	-17.44°C

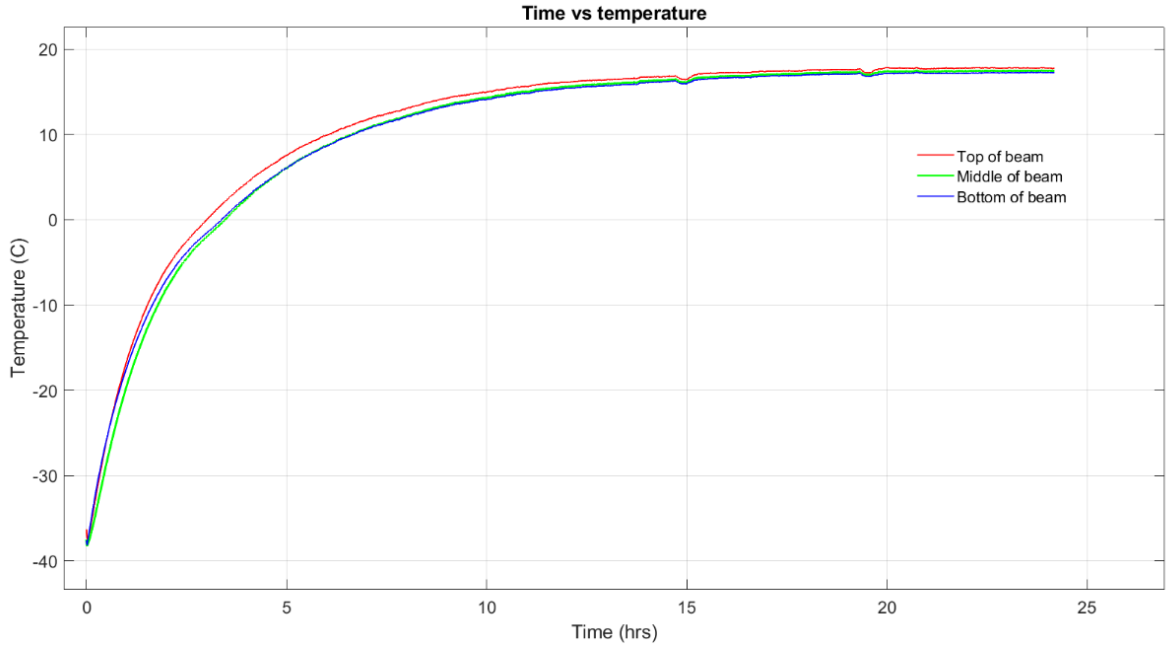

Figure 48. Time vs. temperature data of beam after removing from cold room.

Evaluating the temperature change data after removing the beam from the cold room, it was shown that the beam warmed up rather quickly. In only 15 minutes, the beam had warmed up nearly 7ºC and in 30 minutes, the increase in temperature was over 12ºC. These results made it evident that the test series beams should be tested in the cold room. Although this would require more set-up time and additional logistical requirements, the decision would allow for overall ease of testing and would ensure the beams are tested at the planned temperature.

APPENDIX C

ADDITIONAL BEAM TEST

Appendix C is devoted to a discussion on an additional beam test performed during this research. After initial testing, the SBLTRT beam results were not as predicted and performed lowest among the room temperature beams (with respect to ultimate capacity and stiffness). Unlike other beams, pre-loading occurred while testing this beam and this was thought to potentially have had a negative effect on the results. After starting the SBLTRT beam test and applying load until 4.96 kips, it was found that the strain gauge was not working. The beam was then unloaded, and the test was restarted after fixing the strain gauge problem. The 4.96 kips load is much higher than, 260% of, the load required for the cracking moment (1.91 kips from Table 15) of that beam which was calculated as 2.87 kip-ft. Additionally, from Figure 27, it can be seen that all the load-displacement curves of the beams in this study change their slopes sometime between 2-4 kips loading and the load displacement behavior no longer remains linear afterwards. Therefore, it was concluded here that the pre-loading was most likely the reason for observing the unexpected results for the SBLTRT beam and it was decided to construct and test another beam.

One replacement beam of SBLTRT was constructed and tested following the same procedures as the previous beams. The slump value of the mix was 3 inches and the average concrete compressive strengths of the replacement beam (SBLTRTA) were 3.58 ksi, 5.09 ksi and 5.10 ksi for 7, 28 and 35 days, respectively. The calculated normalized factor for the beam was 0.981 which was calculated following the process previously shown in Table 16.

The comparison between all room temperature beams, including SBLTRTA, is shown in Figure 49. From the figure, it can be seen that once again the SBLTRTA beam did not reach the desired results, and actually performed below the original SBLTRT. These results were unexpected, and it seemed as though the epoxy resin had no or very little contribution to the beam

capacity, because initially the curve follows the counterpart control beam (CBRT) almost identically. There was no pre-loading issue for this new test and because the only difference from the new beam and the first batch of beams was timing (two months between casting and testing), the researchers decided to dig into the possible effects of timing/shelf life on the particular epoxy resin used here.

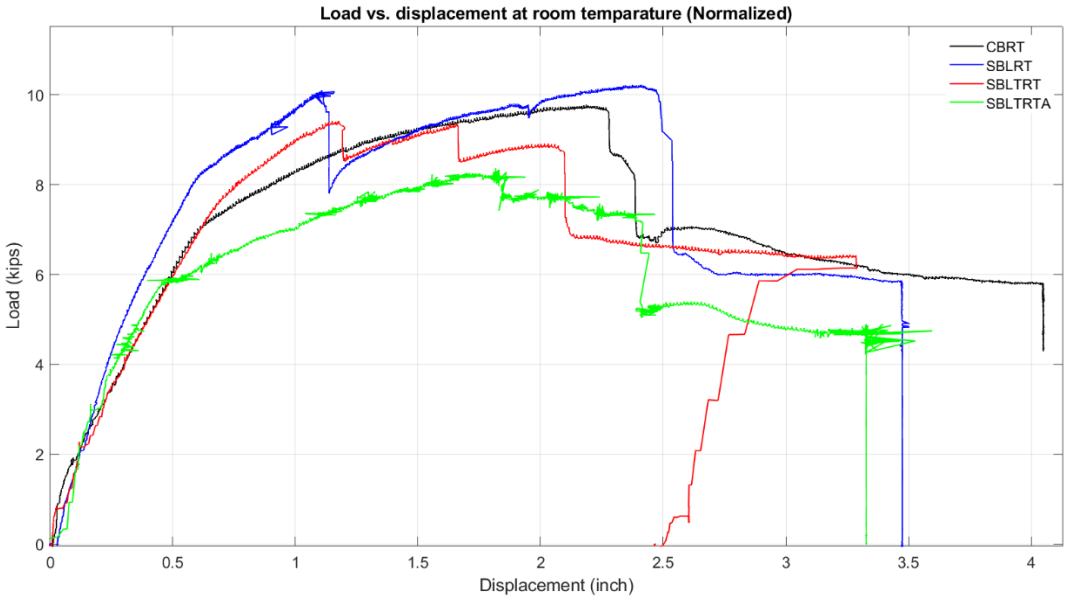

Figure 49. Load vs. mid span displacement of all room temperature beams.

After having a conversation with the manufacturer (FibreGlast) and doing some research on this issue, the (presumed) reason behind the SBLTRTA beam behavior can be summarized as the epoxy resin having reduced properties over time. The epoxy resin was applied to the SBLTRTA beam two months after applying epoxy resin to the other beams and at around six months after initially opening the epoxy resin containers (when the FRP coupons were constructed). The manufacturer did not have any specific data for the exact shelf life of the epoxy resin since that depends on several variables; however, it is known that epoxy resin can have reduced properties if it crystalizes over time or possibly because of storage conditions. The crystallization of epoxy

resin can be identified visually when it gets thicker and cloudy (see Figure 50 (a)). Sometimes, depending on several factors, the crystallization can be "treated" by simply heating up the fluid, which was done for the resin shown in Figure 50 (b). Figure 51 shows the epoxy resin used in the SBLTRTA beam construction and it can clearly be seen that the epoxy resin had crystalized. The resin may possibly be restored by heating it to 120-130°F and stirring until the crystals have resolved; however, because of the timing of this study, another beam has not been constructed and the SBLTRTA beam result is discarded. Although the SBLTRT beam had the preloading issue, it follows other trends and was therefore included and discussed in the Experimental Results and Discussion of Results sections of Chapter 5.

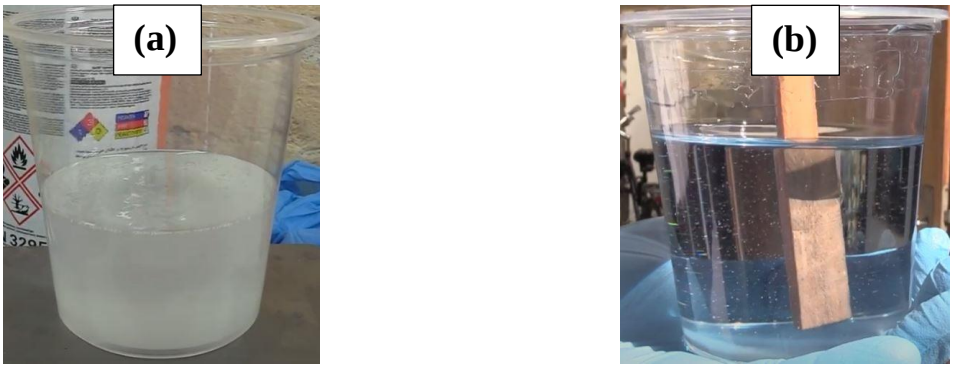

Figure 50. Epoxy resin; (a) Crystalized, (b) After removing crystallization. (Andrés Chavarria YouTube channel).

Figure 51. Epoxy resin used in this study for the SBLTRTA beam.